7

CRYSTAL-FIELD EXCITATIONS IN THE LIGHT RARE EARTHS

A magnetic ion in a rare earth metal experiences a crystalline electric field from the surroundings, which gives rise to an overall splitting of the order 10–20 meV of the ionic ground-state J-multiplets. Crystal-field excitations are collective normal modes of the system, associated with transitions between the different levels of the ground-state multiplets. Even though there is an obvious qualitative difference between the crystal-field excitations in paramagnetic Pr and the spin waves in the isotropic ferromagnet Gd, it is not in general easy to give a precise prescription for differentiating between the two types of excitation. The spin-wave modes are derived from the precession which the moments execute when placed in a magnetic field. The two transverse components of a single moment change in time in a correlated fashion in such a precession, and this *phase-locking* is only possible when the time-reversal symmetry is broken. Hence the spin waves may be considered as the magnetic excitations related to the broken time-reversal symmetry of a magnetically ordered phase. However, spin waves may exist in the paramagnetic phase in the vicinity of the phase transition, if the time-reversal symmetry is broken locally. In the ordered phase, there may be additional magnetic excitations, associated either with the longitudinal fluctuations of the moments, or with further transitions between the MF levels, made possible by a strong mixing of the $|J_z>$-states in the crystal field, as discussed in Section 5.3.2. Depending on the circumstances, these additional excitations may be named crystal-field or molecular-field excitations. The effects of the crystal field, relative to that of the exchange field, are important in the four heavy rare earths Tb – Er, but not sufficiently to produce other well-defined magnetic excitations, in addition to the spin waves. In their paramagnetic phases, the temperature is sufficiently high, compared with the crystal-field splittings, that potential crystal-field excitations have such low intensity, and are so damped, as to be unobservable. Among the rare earth metals, crystal-field excitations are consequently only found in the light half of the series, and in Tm (McEwen *et al.* 1991) where, as discussed in the previous section, the crystal-field effects are relatively stronger because of the de Gennes scaling of the exchange.

We shall therefore concentrate our discussion on Pr, the paradigm

of crystal-field systems. We begin by using the RPA to analyse a number of model systems which, though oversimplified, contain much of the essential physics of the magnetic excitations, sometimes known as *magnetic excitons*, observed on both the hexagonal and the cubic sites in Pr. In the following section, it is shown how effects neglected in the RPA modify the *energies* and *lifetimes* of these excitations. The perturbations of the crystal-field system by the *lattice*, the *conduction electrons*, and the *nuclei* are then considered. This discussion is largely parallel to that of spin-wave systems in Chapter 5; the magnetoelastic interactions couple the phonons to the magnetic excitations and modify the elastic constants, and the conduction electrons limit the lifetimes of the excitations, especially at small q, while themselves experiencing a substantial increase in effective mass. The major effect of the *hyperfine interaction* has no counterpart in spin-wave systems, however, since it is able to induce *collective electronic–nuclear ordering* at low temperatures, and hence affect all magnetic properties drastically. Because the hexagonal sites in Pr constitute an *almost-critical system*, relatively small perturbations are able to drive it into a magnetically-ordered state. The effect of the *internal* interactions with the nuclei and magnetic impurities, and *external* perturbations by uniaxial stress or a magnetic field, are considered. Finally, we discuss a number of specific aspects of the magnetic excitations in Pr, in the paramagnetic and ordered phases.

7.1 MF-RPA theory of simple model systems

The general procedure for calculating the RPA susceptibility was outlined in Section 3.5. If we consider the Hamiltonian

$$\mathcal{H} = \sum_i \mathcal{H}_{\mathrm{J}}(\mathbf{J}_i) - \frac{1}{2}\sum_{ij} \mathbf{J}_i \cdot \overline{\overline{\mathcal{J}}}(ij) \cdot \mathbf{J}_j, \qquad (7.1.1)$$

which includes a general two-ion coupling between the dipolar moments, and assume the system to be in the paramagnetic state, we find the RPA susceptibility to be

$$\overline{\overline{\chi}}(\mathbf{q},\omega) = \left\{ 1 - \overline{\overline{\chi}}^{\,o}(\omega)\overline{\overline{\mathcal{J}}}(\mathbf{q}) \right\}^{-1} \overline{\overline{\chi}}^{\,o}(\omega), \qquad (7.1.2)$$

which is a simple generalization of eqn (3.5.8), as in (6.1.7). The essence of the problem therefore lies in the calculation of the non-interacting susceptibility $\overline{\overline{\chi}}^{\,o}(\omega)$, as determined by the single-ion Hamiltonian $\mathcal{H}_{\mathrm{J}}(\mathbf{J}_i)$. In the case of a many-level system, where J is large, this normally requires the assistance of a computer. Analytical expressions for $\overline{\overline{\chi}}(\mathbf{q},\omega)$ may, however, be obtained for systems where the number of crystal-field levels is small, i.e. between 2–4 states corresponding to $J = \frac{1}{2}$, 1, or $\frac{3}{2}$. Such small values of J are rare, but the analysis of these models is also

useful for systems with larger J, if the higher-lying levels are not coupled to the ground state, and are so sparsely populated that their influence is negligible. According to *Kramers' theorem*, the states are at least doubly degenerate in the absence of an external magnetic field, if $2J$ is odd. In order to construct simple models with relevant level-schemes, we may consider a *singlet–singlet* or a *singlet–triplet* configuration, instead of systems with $J = \frac{1}{2}$ or $J = \frac{3}{2}$. These models may show some unphysical features, but these do not normally obscure the essential behaviour.

The simplest level scheme is that of the singlet–singlet model. This may be realized conceptually by lifting the degeneracy of the two states with $J = \frac{1}{2}$ with a magnetic field, and then allowing only one of the components of **J** perpendicular to the field to interact with the neighbouring ions. This is the so-called *Ising model in a transverse field*. Assuming the coupled components to be along the α-axis, we need only calculate the $\alpha\alpha$-component of $\overline{\overline{\chi}}^{\,o}(\omega)$. The lower of the two levels, at the energy E_0, is denoted by $|0>$, and the other at E_1 by $|1>$. The single-ion population factors are n_0 and n_1 respectively, and the use of eqn (3.5.20) then yields

$$\chi_{\alpha\alpha}^{o}(\omega) = \frac{2n_{01}M_\alpha^2\Delta}{\Delta^2 - (\hbar\omega)^2}, \tag{7.1.3}$$

where $M_\alpha = |<0|J_\alpha|1>|$ is the numerical value of the matrix element of J_α between the two states, while the two other (elastic) matrix elements are assumed to be zero. $\Delta = E_1 - E_0$ is the energy difference, and $n_{01} = n_0 - n_1$ is the difference in population between the two states. From eqn (7.1.2), we have immediately, since only $\mathcal{J}_{\alpha\alpha}(\mathbf{q})$ is non-zero,

$$\chi_{\alpha\alpha}(\mathbf{q},\omega) = \frac{2n_{01}M_\alpha^2\Delta}{E_{\mathbf{q}}^2 - (\hbar\omega)^2}, \tag{7.1.4a}$$

where the *dispersion relation* is

$$E_{\mathbf{q}} = \left[\Delta\big\{\Delta - 2n_{01}M_\alpha^2\mathcal{J}_{\alpha\alpha}(\mathbf{q})\big\}\right]^{1/2}. \tag{7.1.4b}$$

These excitations are actually spin waves in this case of extreme axial anisotropy, but they have all the characteristics of crystal-field excitations. The energies are centred around Δ, the energy-splitting between the two levels, and the bandwidth of the excitation energies, due to the two-ion interaction, is proportional to the square of the matrix element, and to the population difference, between them. These factors also determine the neutron-scattering intensities which, from (3.2.18) and (4.2.3), are proportional to

$$\begin{aligned}
\mathcal{S}_d^{\alpha\alpha}(\mathbf{q},\omega) &= \frac{1}{1 - e^{-\beta\hbar\omega}}\frac{n_{01}M_\alpha^2\Delta}{E_{\mathbf{q}}}\big\{\delta\big(\hbar\omega - E_{\mathbf{q}}\big) - \delta\big(\hbar\omega + E_{\mathbf{q}}\big)\big\} \\
&\simeq M_\alpha^2\frac{\Delta}{E_{\mathbf{q}}}\big\{n_0\delta\big(\hbar\omega - E_{\mathbf{q}}\big) + n_1\delta\big(\hbar\omega + E_{\mathbf{q}}\big)\big\}.
\end{aligned} \tag{7.1.5}$$

The approximate expression is obtained by using $\hbar\omega \simeq \pm\Delta$ in the temperature denominator.

The above results are only valid as long as the excitation energies remain positive for all $\mathbf{q}$. The mode of lowest energy is found at the wavevector $\mathbf{Q}$ at which $\mathcal{J}_{\alpha\alpha}(\mathbf{q})$ has its maximum. Introducing the critical parameter

$$R(T) = 1 - \frac{\chi^{o}_{\alpha\alpha}(0)}{\chi_{\alpha\alpha}(\mathbf{Q},0)}, \qquad (7.1.6a)$$

which, in the present approximation, depends on T through n_{01}:

$$R(T) = 1 - \left(E_{\mathbf{Q}}/\Delta\right)^2 = n_{01}R_0 \qquad ; \qquad R_0 = \frac{2M_\alpha^2 \mathcal{J}_{\alpha\alpha}(\mathbf{Q})}{\Delta}, \quad (7.1.6b)$$

we find that the excitation energies are all positive as long as $R(T) < 1$. This parameter increases monotonically when the temperature is lowered and, if the zero-temperature value R_0 is greater than one, the energy $E_{\mathbf{Q}}$ of the *soft mode* vanishes at a temperature $T = T_N$ (or T_C if $\mathbf{Q} = \mathbf{0}$) determined by $R(T_N) = 1$. Correspondingly, the susceptibility $\chi_{\alpha\alpha}(\mathbf{Q},0)$ becomes infinite at this temperature. This indicates that the system undergoes a second-order phase transition, from a paramagnetic phase to one which has the same symmetry as the soft mode. In this case, this means that $\langle J_{\alpha i}\rangle = \langle J_\alpha\rangle \cos\left(\mathbf{Q}\cdot\mathbf{R}_i + \varphi\right)$, where the MF equations have a non-zero solution for $\langle J_\alpha\rangle$ below, but not above, T_N.

We shall assume ferromagnetic ordering with $\mathbf{Q} = \mathbf{0}$. For the Ising model in a transverse field, the development of a ferromagnetic moment below T_C corresponds to a rotation of the moments away from the direction of the 'transverse field'. The MF Hamiltonian in the $(|0> |1>)$-basis is

$$\mathcal{H}_{\mathrm{MF}}(i) = \begin{pmatrix} E_0 & -\delta \\ -\delta & E_1 \end{pmatrix} \qquad ; \qquad \delta = M_\alpha \mathcal{J}_{\alpha\alpha}(\mathbf{0})\langle J_\alpha\rangle. \qquad (7.1.7)$$

Introducing the new eigenstates

$$\begin{aligned}
|0'> &= \cos\theta|0> + \sin\theta|1> \\
|1'> &= \cos\theta|1> - \sin\theta|0>,
\end{aligned} \qquad (7.1.8a)$$

we find that the coupling parameter δ, due to the molecular field, gives rise to a non-zero moment $<0'|J_\alpha|0'> = M_\alpha \sin 2\theta$ in the ground state. Because it is a singlet, the ground state $|0>$ in the paramagnetic phase is necessarily 'non-magnetic', in zero field. This condition does not apply in the ordered phase, so the nomenclature *induced-moment* system is frequently used. In the ordered phase, the splitting between the two singlets is $\Delta/\cos 2\theta$, and $\langle J_\alpha\rangle = n_{01}M_\alpha \sin 2\theta$ (where n_0 and n_1 are now

the population factors of the new eigenstates). The condition that $\mathcal{H}_{\mathrm{MF}}$ should be diagonal in the new basis requires that

$$\cos 2\theta = \frac{1}{n_{01} R_0}, \qquad (7.1.8b)$$

which only has a solution if $n_{01} R_0 \geq 1$, in accordance with the critical condition $R(T_C) = 1$. The MF susceptibility is

$$\chi^o_{\alpha\alpha}(\omega) = \frac{2n_{01} M^2_\alpha \Delta \cos 2\theta}{(\Delta/\cos 2\theta)^2 - (\hbar\omega)^2} + \beta(n_0 + n_1 - n^2_{01}) M^2_\alpha \sin^2 2\theta \, \delta_{\omega 0}, \ (7.1.9)$$

revealing that there are now two kinds of excitation. The first is a continuation of the paramagnetic inelastic branch, with the dispersion relation

$$E^2_{\mathbf{q}} = \frac{\Delta}{\cos 2\theta} \Big(\frac{\Delta}{\cos 2\theta} - 2n_{01} M^2_\alpha \mathcal{J}(\mathbf{q}) \cos^2 2\theta \Big), \qquad (7.1.10)$$

which is again positive at all wave-vectors, consistent with the stability of the ordered phase. $E_{\mathbf{Q}}$ therefore vanishes when T approaches T_C from above or below, and this kind of second-order phase transition is frequently known as a *soft-mode transition*. In addition to the inelastic mode, there appears a diffusive mode which, within the RPA, is purely elastic. The diffusive mode, but not the inelastic branch, has a parallel in the spectrum of the longitudinal fluctuations of a Heisenberg ferromagnet, described by eqn (3.5.27), since the spectrum analysed here is longitudinal relative to the polarization of the spontaneously ordered moment.

The behaviour discussed above is typical for a system where the crystal-field ground state is a singlet. The most characteristic feature of such a system is that the two-ion coupling must exceed a certain threshold value, relative to the crystal-field splitting, in order to force the system into a magnetically-ordered state at low temperatures. In this case, the condition is that the ratio R_0 must be greater than one. The general (MF) condition is that $\chi^o_{\alpha\alpha}(0)\mathcal{J}_{\alpha\alpha}(\mathbf{Q}) > 1$, for at least one of the α-components, where $\chi^o_{\alpha\alpha}(0)$ is the paramagnetic susceptibility at zero temperature. This condition is a consequence of the fact that the single-ion susceptibility remains finite in the zero-temperature limit, if the ground state is non-degenerate. If the ground state is degenerate, on the other hand, one or more components of the static single-ion susceptibility contains an elastic contribution proportional to $1/k_B T$, and its divergence in the $T = 0$ limit results in an ordering of the moments, within the MF approximation, no matter how weak the two-ion coupling. Fluctuations not included in the MF theory modify the critical

condition for $\mathcal{J}(\mathbf{Q})$, but the qualitative behaviour is unchanged. It is therefore possible to realize a system in which the moments are relatively strongly coupled to each other, but which remains paramagnetic at low temperatures, i.e. a crystal-field system in which cooperative effects are important. Perhaps the best example is elemental Pr, which is only slightly undercritical, with $R_0 \simeq 0.92$, and therefore exhibits a rich variety of unusual magnetic phenomena.

Pr crystallizes in the double hexagonal-close-packed (dhcp) structure, illustrated in Fig. 1.3, with the stacking sequence ABAC along the *c*-axis. This implies that there are two non-equivalent types of site of different symmetry in the crystal. The ions in A layers are in an approximately cubic environment, with nearest neighbours close to the fcc configuration, while those in the B and C layers experience a crystal field of hexagonal symmetry and form together an hcp structure. The tripositive Pr ion, with two $4f$ electrons, is a *non-Kramers* ion ($S = 1$, $L = 5$, and $J = 4$ for the ground-state multiplet) allowing the occurrence of singlet crystal-field states. Experimental observations, particularly of neutron scattering, have revealed that both kinds of site in fact have a singlet as the ground state. The lowest states of the *hexagonal* ions are the singlet $|J_\zeta = 0 >$ followed by the doublet $|J_\zeta = \pm 1 >$, with an energy difference of $\Delta_h \simeq 3.5\,\mathrm{meV}$, as illustrated in Fig. 1.16. If the distortion of the point symmetry of the *cubic* ions, due to the non-ideal c/a ratio, is neglected, their ground state is the Γ_1-singlet, with the Γ_4-triplet lying $\Delta_c \simeq 8.4\,\mathrm{meV}$ above it. A complete survey of the classification and energies of crystal-field states in cubic surroundings has been given by Lea, Leask, and Wolf (1962). The possibility that the Γ_4 state is split into a singlet and a doublet, due to the deviation from cubic symmetry, has not yet been investigated experimentally. At temperatures well below $40\,\mathrm{K}$ ($\sim 3.5\,\mathrm{meV}$), only the two ground states are populated significantly, and Pr may be considered to be a coupled singlet–doublet and singlet–triplet system. Furthermore, the difference between Δ_h and Δ_c is so large, compared to the two-ion interactions, that the excitation spectrum can be divided into two parts, related respectively to the crystal-field transitions on each kinds of ion. The weak coupling of the two components may be accounted for by second-order perturbation theory (Jensen 1976a), leading to an effective decoupling, with the two-ion parameters replaced by slightly different, effective values. Hence, at low temperature, Pr may be treated as a combination of a singlet–doublet system on an hcp lattice and a singlet–triplet system on a simple hexagonal lattice. Of these, the singlet–doublet system is much the more important because of the smaller value of the crystal-field splitting. The singlet–doublet scheme corresponds to an effective $J = 1$ and, if the two doublet states are defined to be $|1_\mathrm{s} > = \big(|+1> + |-1>\big)/\sqrt{2}$

and $|1_\mathrm{a}>= \big(|+1>-|-1>\big)/\sqrt{2}i$, the only non-zero matrix elements of
$\mathbf{J}$ are $<1_\mathrm{a}|J_\zeta|1_\mathrm{S}>= i$ and $<0|J_\xi|1_\mathrm{S}>=<0|J_\eta|1_\mathrm{a}>= \sqrt{J(J+1)/2}$,
plus their Hermitian conjugates. In Pr, the matrix element of J_ζ is a
factor of $\sqrt{10}$ smaller than the other matrix elements. This means that
the transformation of the $(J=4)$ ion of Pr to an effective $J=1$ system
introduces a scaling of the two-ion couplings $\mathcal{J}_{\xi\xi}(\mathbf{q})$ and $\mathcal{J}_{\eta\eta}(\mathbf{q})$ by a
factor of 10, compared to $\mathcal{J}_{\zeta\zeta}(\mathbf{q})$, and the latter may therefore be ne-
glected to a first approximation. Hence the $(J=1)$ XY-model is an
appropriate low-temperature description of the hexagonal ions in Pr.

The RPA theory of the XY-model, in the singlet–doublet case, is
nearly identical to that developed above for the Ising model in a trans-
verse field. One difference is that $n_0 + n_1 + n_2 = n_0 + 2n_1 = 1$, instead
of $n_0 + n_1 = 1$, but since this condition has not been used explicitly (the
population of any additional higher-lying levels is neglected), it may be
considered as accounted for. The other modification of the above results
is that there are now two components of $\overline{\overline{\chi}}(\mathbf{q},\omega)$ which are important:
$\chi^o_{xx}(\omega) = \chi^o_{yy}(\omega)$ are given by the same expression as $\chi^o_{\alpha\alpha}(\omega)$ in eqn
(7.1.3) (with $M_\alpha = 1$ when $J=1$), whereas $\chi^o_{xy}(\omega) \equiv 0$ (the (xyz)-axes
are assumed to coincide with the $(\xi\eta\zeta)$-axes). This means that, for a
Bravais lattice, there are two poles at positive energies in the RPA sus-
ceptibility (7.1.2) at each $\mathbf{q}$-vector. As long as $\mathcal{J}_{xy}(\mathbf{q}) = 0$, one of the
modes describes a time variation of J_x alone, and the other J_y alone,
and their dispersion relations are both given by eqn (7.1.4b), with α set
equal to x or y. It is interesting to compare this result with the spin-
wave case. Although the magnetic response is there also determined by
a 2×2 matrix equation, it only leads to one (spin-wave) pole at posi-
tive energies, independently of whether the two-ion coupling is isotropic.
The cancellation of one of the poles is due to the specific properties of
$\chi^o_{xy}(\omega)$ in (5.1.3), produced by the molecular field (or the broken time-
reversal symmetry) in the ordered phase. In the case considered above,
the two modes may of course be degenerate, but only if $\mathcal{J}_{xx}(\mathbf{q})$ is equal
to $\mathcal{J}_{yy}(\mathbf{q})$. In an hcp system, such a degeneracy is bound to occur, by
symmetry, if $\mathbf{q}$ is parallel to the c-axis. If the degeneracy is lifted by
anisotropic two-ion couplings, which is possible in any other direction in
$\mathbf{q}$-space, the x- and y-modes mix unless $\mathbf{q}$ is parallel to a b-axis. The va-
lidity of the results derived above is not restricted to the situation where
the doublet lies above the singlet. If the XY-model is taken literally,
all the results apply equally well if Δ, and hence also n_{01}, is negative.
However, if the z-components are coupled to some extent, as in Pr, the
importance of this interaction is much reduced at low temperature if Δ
is positive. In this case the zz-response, which is purely elastic,

$$\chi_{zz}(\mathbf{q},\omega) \simeq \chi^o_{zz}(\omega) = 2\beta n_1 \delta_{\omega 0}$$

is frozen out exponentially in the low-temperature limit.

As shown in Fig. 7.1, the dispersion relations for the magnetic excitations on the hexagonal sites in Pr, measured by Houmann *et al.* (1979), illustrate many of the characteristic features of the $(J = 1)$ XY-model. As mentioned above, when $\mathbf{q}$ is along ΓM, the excitations are pure x- or y-modes. The hexagonal ions constitute an hcp structure, so there are an optical and an acoustic mode for each polarization. The excitation energies (7.1.4) are then generalized analogously to eqn (5.1.9), and since $\mathcal{J}_2(\mathbf{0})$ is negative in this case, the lower two branches are the optical modes. From intensity measurements of the type illustrated in Fig. 4.2, it may readily be deduced that the lowest branch is the longitudinal optical y-mode. The experimental dispersion relations show clearly that $\mathcal{J}_{xx}(\mathbf{q})$ and $\mathcal{J}_{yy}(\mathbf{q})$ have very different dependences on wave-vector, and that the anisotropic component is a substantial fraction of the two-ion coupling.
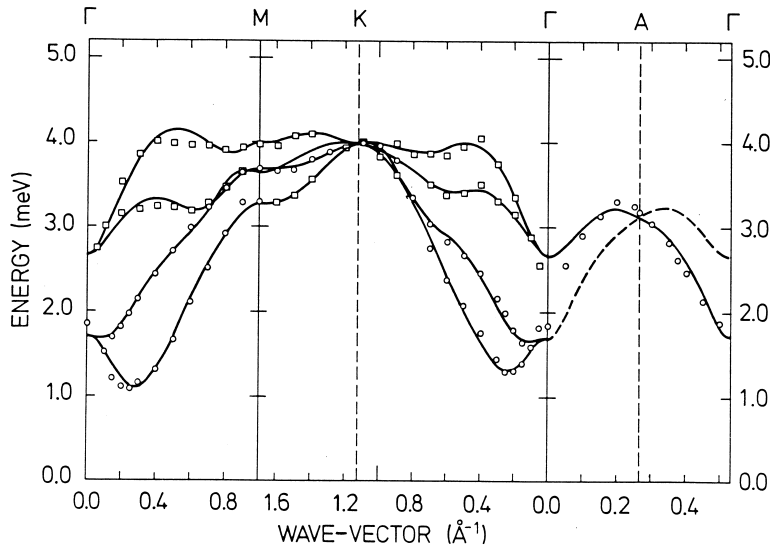

Fig. 7.1. Dispersion relations for the magnetic excitations propagating on the hexagonal sites of Pr at 6 K. In the basal plane, the squares and circles denote the experimental results for the acoustic and optical modes respectively. The double degeneracy of these excitations is lifted by anisotropic exchange, and the lower and upper branches correspond respectively to polarizations predominantly parallel and transverse to the wave-vector. The double-zone representation is used for the ΓA direction, along which the two transverse excitations are degenerate by symmetry, and therefore form a single branch.

The singlet–triplet model, relevant in the case of cubic symmetry and, with some modifications, also for the cubic ions in Pr, introduces one new feature; each component of the single-ion susceptibility includes a mixture of an elastic and an inelastic response. In surroundings with cubic symmetry, $\overline{\overline{\chi}}^{\,o}(\omega)$ is proportional to the unit tensor, and the diagonal component is

$$\chi^{\,o}(\omega) = \frac{2n_{01}M_1^2\Delta}{\Delta^2 - (\hbar\omega)^2} + 2\beta n_1 M_2^2 \delta_{\omega 0}, \qquad (7.1.11)$$

where now $n_0 + 3n_1 = 1$. This result follows from the circumstance that J_x, for instance, has a matrix element between the singlet state and one of the triplet states, and a matrix element between the two other triplet states, the numerical values of which are denoted by M_1 and M_2 respectively. In the $\Gamma_1 - \Gamma_4$ case with $J = 4$, corresponding to Pr, $M_1 = \sqrt{20/3}$ and $M_2 = 1/2$. The inelastic $\chi(\mathbf{q}, \omega \neq 0)$ is equivalent to (7.1.4) for the singlet–singlet system, but with M_α replaced by M_1. Because of the elastic contribution, the critical condition $R(T_N) = 1$ is now determined from

$$R(T) = \big(2n_{01}M_1^2 + 2\beta\Delta n_1 M_2^2\big)\frac{\mathcal{J}_{\alpha\alpha}(\mathbf{Q})}{\Delta}. \qquad (7.1.12)$$

The inelastic neutron-scattering spectrum is also determined by eqn (7.1.4) with $M_\alpha = M_1$ and $\alpha = x$, y, or z, when the off-diagonal coupling is neglected. The only difference is that there may now be three different branches, depending on the polarization. In addition to the inelastic excitations, the spectrum also includes a diffusive, elastic mode. In order to determine its contribution to the scattering function, $\delta_{\omega 0}$ in (7.1.11) may be replaced by $\delta^2/\{\delta^2 - (\hbar\omega)^2\}$, and if the limit $\delta \to 0$ is taken at the end, the result is found to be:

$$\mathcal{S}_d^{\alpha\alpha}(\mathbf{q}, \omega \approx 0) = \frac{\chi^{\,o}(0) - \chi^{\,o}(\omega \to 0)}{\beta\{1 - \chi^{\,o}(\omega \to 0)\mathcal{J}_{\alpha\alpha}(\mathbf{q})\}\{1 - \chi^{\,o}(0)\mathcal{J}_{\alpha\alpha}(\mathbf{q})\}}\delta(\hbar\omega)$$

$$= 2n_1 M_2^2 \left(\frac{\Delta}{E_\mathbf{q}}\right)^2 \frac{\chi_{\alpha\alpha}(\mathbf{q}, 0)}{\chi^{\,o}(0)}\,\delta(\hbar\omega). \qquad (7.1.13)$$

The two-ion coupling is assumed to be diagonal, and $\chi^{\,o}(\omega \to 0)$ is the static susceptibility without the elastic contribution. The scattering function at $\mathbf{q} = \mathbf{Q}$, integrated over small energies, diverges when T approaches T_N, as it also does in the singlet–singlet system. In the latter case, and in the singlet–doublet system, the divergence is related to the softening of the inelastic mode ($E_\mathbf{Q} \to 0$ when $T \to T_N$), as in eqn (7.1.5). In the singlet–triplet system, it is the intensity of the

elastic, diffusive mode which diverges, whereas the intensity of the inelastic mode stays finite and its energy is still non-zero at the transition. Within the simple MF-RPA theory, the critical behaviour has changed, because of the elastic term in the crystal-field susceptibility, so that the transition is no longer accompanied by a soft mode. The energy of the inelastic mode at $\mathbf{q} = \mathbf{Q}$, when T is close to T_N, depends on Δ and on how large the elastic term is at the transition. If this elastic contribution is small, the energy of the inelastic mode may be so small that it becomes overdamped because of the influence of the critical fluctuations, and therefore indistinguishable from the divergent diffusive peak. However, if the inelastic mode is sufficiently separated in frequency from the low-frequency critical fluctuations, it may persist as a reasonably well-defined excitation even near the phase transition.

The dhcp structure of Pr has four atoms per unit cell, so there are four branches of the dispersion relation for each polarization. If the hexagonal and cubic sites are decoupled, these decompose into two sets, each comprising two modes, which may be described as acoustic and optical, propagating on the sites of a particular symmetry. The complementary excitations to those of Fig. 7.1 propagate on the cubic sites, and their dispersion relations, also studied by Houmann *et al.* (1979), are illustrated in Fig. 7.2. If the hexagonal sites are ignored, the cubic sites lie on a simple hexagonal lattice, so that a double zone may be
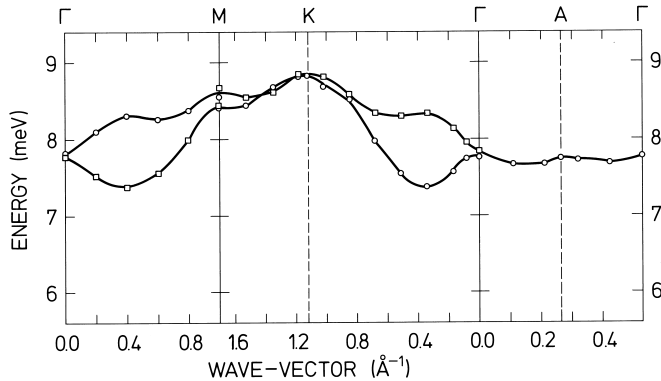

Fig. 7.2. Dispersion relations for the excitations propagating on the cubic sites of Pr at 6 K, plotted in the Brillouin zone of the dhcp structure. The upper and lower branches in the basal plane are respectively the acoustic and optical modes. The polarization vector of these excitations is perpendicular to the *c*-axis. In contrast to Fig. 7.1, no splitting of these branches by anisotropic two-ion coupling is observed, within the experimental resolution of about $0.5\,\mathrm{meV}$.

used. However, it is both more convenient and, in general, more correct to use the true Brillouin zone for the dhcp structure, as in Fig. 7.2. The excitations in this figure are polarized in the plane, and may also be described by (7.1.4), with parameters appropriate to the cubic sites. The z-modes were not observed in these experiments, on account of the neutron scans employed. The dispersion is much smaller than that on the hexagonal sites and, in particular, it is negligible in the c-direction, indicating very weak coupling between planes of cubic ions normal to this axis. Again in contrast to the hexagonal ions, the splitting between modes of different polarization is not resolved, demonstrating that the anisotropy in the two-ion coupling is smaller.

7.2 Beyond the MF-RPA theory

When the temperature is raised, the available magnetic scattering intensity, from eqn (4.2.7) proportional to $J(J+1)$, is divided more and more equally among the $(2J)!$ different dipolar transitions, and in the high-temperature limit half the intensity is transferred to the emissive part of the spectrum. This means that the different crystal-field excitations become weaker and less dispersive, and correspondingly correlation effects become less important as the temperature is raised. An additional mechanism diminishing the correlation effects at elevated temperatures is the scattering of the excitations against random fluctuations, neglected in the MF-RPA theory. In this theory, all the ions are assumed to be in the same MF state, thus allowing an entirely coherent propagation of the excitations. However, at non-zero temperatures, the occupations of the different crystal-field levels differ from site to site, and these *single-site fluctuations* lead to a non-zero linewidth for the excitations. In fact, if two-ion interactions are important, such fluctuations already exist at zero temperature, as the MF ground state $\prod_i |0_i>$ cannot be the true ground state, because $\sum_i |0_i><0_i|$ does not commute with the two-ion part of the Hamiltonian. Hence, the occupation n_0 of the 'ground-state' is reduced somewhat below 1 even at $T = 0$. The response functions derived above already predict such a reduction of n_0 but, as discussed earlier in connection with eqn (3.5.23), the MF-RPA theory is not reliable in this order. A more satisfactory account of the influence of fluctuations, both at zero and non-zero temperatures, can only be obtained by calculations which go beyond the MF-RPA.

One way to proceed to higher order is to postpone the use of the RPA decoupling to a later stage in the Green-function hierarchy generated by the equations of motion. Returning to our derivation of the MF-RPA results in Section 3.5; instead of performing the RPA decoupling on the Green function $\langle\langle a_{\nu\xi}(i)a_{\nu'\mu'}(j)\,;\,a_{rs}(i')\rangle\rangle$, as in eqn (3.5.16), we first apply this decoupling to the higher-order Green functions appearing in

the equation of motion of this function. This method requires rather extensive manipulation, but it is essentially straightforward, and we shall not discuss the details here. It has been applied to the $(J = 1)$-model, corresponding to Pr (Jensen 1982b), and the results may be interpreted by replacing the crystal-field splitting and the exchange coupling by renormalized quantities, while the excitations acquire a linewidth proportional to the fluctuations in the single-site population factors. As may be seen in Fig. 7.3, this *self-consistent RPA* gives a good account of the temperature dependence of the excitations on the hexagonal sites in Pr, and fits the results of Houmann *et al.* (1975b) somewhat better than their MF model. The mode of lowest energy varies very rapidly with
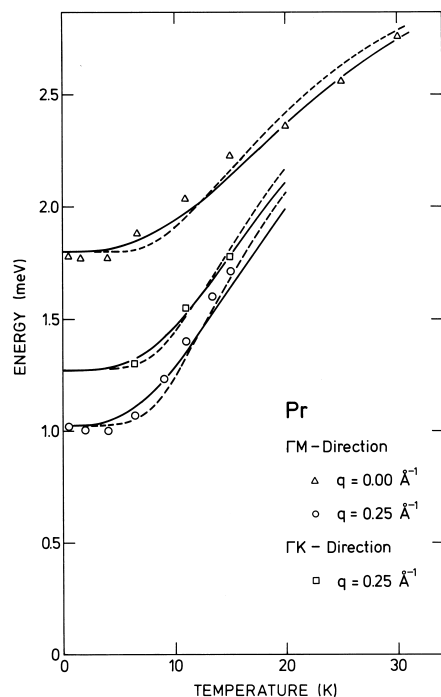

Fig. 7.3. The temperature dependence of the excitation energies at three different wave-vectors for the hexagonal sites in Pr. The dashed lines give the results of a MF calculation, and the full curves are based on the self-consistent RPA. The lowest-lying mode is the incipient soft mode, whose **q** and longitudinal polarization correspond to the antiferromagnetic structure which may be induced in Pr by various perturbations.

temperature, but does not become soft, so Pr remains paramagnetic down to very low temperatures. However, these calculations indicate that $R_0 \simeq 0.92$, so that the exchange is very close to the critical value which would drive this *incipient soft mode* to zero energy. As we shall discuss in Section 7.4.1, under these circumstances a variety of perturbations may induce magnetic ordering.

A more elegant technique for obtaining such results is based on a diagrammatic-expansion technique. The introduction of this method requires a further development and refinement of the mathematical analysis of the Green functions, which falls outside the scope of this book. Nevertheless, we wish to discuss some essential problems connected with the use of the technique for rare earth systems, so we will present it very briefly and refer to the books by Abrikosov *et al.* (1965), Doniach and Sondheimer (1974), and Mahan (1990) for more detailed accounts.

Instead of the *retarded* Green function, introduced in eqn (3.3.12), we consider the Green function defined as the τ-ordered ensemble average: $G_{BA}^{\tau}(\tau_1 - \tau_2) \equiv -\langle T_\tau \hat{B}(\tau_1)\hat{A}(\tau_2)\rangle$. Here $\hat{B}(\tau)$ is the equivalent of the time-dependent operator in the Heisenberg picture, eqn (3.2.1), with t replaced by $-i\hbar\tau$. The τ-ordering operator T_τ orders subsequent operators in a sequence according to decreasing values of their τ-arguments, i.e. $T_\tau \hat{B}(\tau_1)\hat{A}(\tau_2) = \hat{B}(\tau_1)\hat{A}(\tau_2)$ if $\tau_1 \geq \tau_2$ or $\hat{A}(\tau_2)\hat{B}(\tau_1)$ otherwise. Restricting ourselves to considering the Green function $G_{BA}^{\tau}(\tau)$ only in the interval $0 \leq \tau \leq \beta$, where $\beta = 1/k_B T$, we may represent it by a Fourier series (corresponding to letting the function repeat itself with the period β):

$$G_{BA}^{\tau}(\tau) = -\langle T_\tau \hat{B}(\tau)\hat{A}\rangle = \frac{1}{\beta}\sum_n G_{BA}^{\tau}(i\omega_n)\,e^{-i\hbar\omega_n\tau} \qquad ; \qquad \hbar\omega_n = \frac{2\pi n}{\beta}.$$
$$(7.2.1a)$$

n is an integer and the ω_n are called the *Matsubara frequencies*. The Fourier coefficients are determined by

$$G_{BA}^{\tau}(i\omega_n) = \int_0^\beta G_{BA}^{\tau}(\tau)\,e^{i\hbar\omega_n\tau}d\tau. \qquad (7.2.1b)$$

The most important property of the τ-ordered Green function is that it can be calculated by perturbation theory using the *Feynman–Dyson* expansion. By dividing the Hamiltonian into two parts, $\mathcal{H} = \mathcal{H}_0 + \mathcal{H}_1$, and denoting the ensemble average with respect to the 'unperturbed' Hamiltonian $\mathcal{H}_0$ by an index '0', it can be shown that

$$G_{BA}^{\tau}(\tau) = -\frac{\langle T_\tau U(\beta,0)\hat{B}(\tau)\hat{A}(0)\rangle_0}{\langle U(\beta,0)\rangle_0}, \qquad (7.2.2a)$$

where

$$U(\beta, 0) = 1 - \int_0^\beta \mathcal{H}_1(\tau_1) d\tau_1 + \cdots$$

$$\cdots + \frac{(-1)^n}{n!} \int_0^\beta \cdots \int_0^\beta T_\tau \mathcal{H}_1(\tau_1) \cdots \mathcal{H}_1(\tau_n) d\tau_1 \cdots d\tau_n + \cdots \quad (7.2.2b)$$

which is suitable for a diagrammatic representation in which the denominator in $(7.2.2a)$ just eliminates all 'un-linked' diagrams. Furthermore, it can be shown that the retarded Green function is the analytic continuation of the τ-ordered function to the real axis in the complex ω-plane, or

$$\chi_{BA}(\omega) = -\lim_{\epsilon \to 0^+} G^\tau_{BA}(i\omega_n \to \omega + i\epsilon), \qquad (7.2.3)$$

and we shall therefore use the frequency arguments $i\omega_n$ and ω to distinguish between respectively the τ-ordered and the retarded Green function.

Considering the simplest case of the Ising model, we wish to calculate the Fourier transform of $G(ij, \tau) = -\langle T_\tau J_{i\alpha}(\tau) J_{j\alpha}\rangle$. We take $\mathcal{H}_0$ to be the single-ion crystal-field Hamiltonian, and the perturbation $\mathcal{H}_1$ is then the two-ion part. With this partition, the ensemble average $\langle\ \rangle_0$ of a product of operators belonging to different sites is just the product of the averages of the operators, i.e. $\langle J_{i\alpha} J_{j\alpha}\rangle_0 = \langle J_{i\alpha}\rangle_0 \langle J_{j\alpha}\rangle_0$ if $i \neq j$. This concentrates attention on the Green function for a single site $G(ii, i\omega_n)$, for which the perturbation expansion leads to a series corresponding to that considered in the CPA calculation, eqn (5.6.9). The only differences are that $\overline{\overline{K}}(i, \omega)$ is replaced by the $\alpha\alpha$-component $K(i\omega_{n'})$ and, more significantly, that the products $(c_i \chi^o(\omega))^p = c_i (\chi^o(\omega))^p$ are replaced by the $2p$th order *cumulant* averages or *semi-invariants*

$$\mathcal{S}^{(2p)} = \frac{1}{\beta^p} \int_0^\beta d\tau_1 \cdots \int_0^\beta d\tau_{2p} \Big\langle T_\tau \prod_{l=1}^{2p} J_{i\alpha}(\tau_l) \Big\rangle_0 \prod_{l=1}^{2p} \exp\big(i\hbar\omega_{nl}\tau_l\big), \quad (7.2.4)$$

with the conditions $\sum_l \omega_{nl} = 0$ and $\omega_{n1} = \omega_n$. The lowest-order semi-invariant is $\mathcal{S}^{(2)} = -g(i\omega_n) = 2n_{01}M_\alpha^2\Delta/\big[\Delta^2 - (i\hbar\omega_n)^2\big]$, which is the Fourier transform of $\langle T_\tau J_{i\alpha}(\tau) J_{i\alpha}\rangle_0$, and $-g(i\omega_n \to \omega) = -g(\omega) = \chi^o(\omega)$. The calculation of the fourth- and higher-order cumulants is more involved. It is accomplished basically by utilizing the invariance of the trace (i.e. of the ensemble average) to a cyclic permutation of the operators, as is discussed, for instance, by Yang and Wang (1974) and Care and Tucker (1977). If the operators are proportional to Bose operators this results in *Wick's theorem*, which here implies that $\mathcal{S}^{(2p)}_{\text{Bose}} = \big[\mathcal{S}^{(2)}\big]^p$. The determination of the cumulant averages is facilitated by

expressing the angular-momentum components as linear combinations of the standard-basis operators introduced by eqn (3.5.11). These are not Bose operators, so the 'contractions' determined by the commutators of the different operators are not c-numbers, but operators which give rise to new contractions. In the singlet–singlet Ising model, the result is

$$
\begin{aligned}
G(ii, i\omega_n) &= G(i\omega_n) = g(i\omega_n) \\
&- \frac{1}{n_{01}^2}\left[(n_0 + n_1)g(i\omega_n)K(i\omega_n) + \frac{1}{\beta}\sum_{n'} g(i\omega_{n'})K(i\omega_{n'})u(n, n')\right]g(i\omega_n) \\
&+ \cdots
\end{aligned}
\tag{7.2.5a}
$$

with

$$
u(n, n') = \frac{g(i\omega_n)}{M_\alpha^2} + \frac{g(i\omega_{n'})}{M_\alpha^2}\frac{(i\hbar\omega_{n'})^2 + \Delta^2}{2\Delta^2} + \tfrac{1}{2}\left(n_0 + n_1 - n_{01}^2\right)\beta.
\tag{7.2.5b}
$$

The sum over the Matsubara frequencies may be transformed into an integral over real frequencies, but it may be advantageous to keep the frequency sum in numerical calculations. Before proceeding further, we must clarify a few points. The first is that $\mathcal{H}_1$ cannot, in general, be consider as being 'small' compared to $\mathcal{H}_0$. However, each time a term involving the two-ion coupling is summed over $\mathbf{q}$, we effectively gain a factor $1/Z$, where Z is the co-ordination number. Hence, if we use $1/Z$ as a small expansion parameter, the order of the different contributions may be classified according to how many $\mathbf{q}$-summations they involve. In the equation above, $K(i\omega_{n'})$ is derived from one summation over $\mathbf{q}$, as in (5.6.17), so the series can be identified as being equivalent to an expansion in $1/Z$. The second point to realize is that it is of importance to try to estimate how the expansion series behaves to infinite order. A truncation of the series after a finite number of terms will produce a response function with incorrect analytical properties. If we consider the corresponding series determining $G(\mathbf{q}, i\omega_n)$, it is clear that any changes in the position of the poles, i.e. energy changes and linewidth phenomena, are reflected throughout the whole series, whereas a (small) scaling of the amplitude of the response function, which might be determined by the first few terms, is not particularly interesting. In other words, what we wish to determine is the first- (or higher-) order correction in $1/Z$ to the denominator of the Green function, i.e. to determine the self-energy $\Sigma(\mathbf{q}, i\omega_n)$, defined by

$$
G(\mathbf{q}, i\omega_n) = \frac{g(i\omega_n)}{1 + g(i\omega_n)\{\mathcal{J}_{\alpha\alpha}(\mathbf{q}) + \Sigma(\mathbf{q}, i\omega_n)\}},
\tag{7.2.6}
$$

assuming the MF-RPA response function to be the starting point. A systematic prescription for calculating the Green function to any finite

order in $1/Z$ has been given by Stinchcombe (1973), see also Vaks *et al.*
(1968). The zero-order result is obtained by the 'boson' approximation
$\mathcal{S}^{(2p)} \simeq [\mathcal{S}^{(2)}]^p$. As is apparent from (7.2.5a), this corresponds to the
replacement of the second and subsequent terms on the r.h.s. by the in-
finite series generated by $-g(i\omega_n)K(i\omega_n)G(i\omega_n)$, leading to an equation
for the single-site Green function which is the equivalent to the *Dyson
equation* for bosons (or fermions), or to the CPA equation with $c = 1$.
The **q**-dependent Green function may be obtained from the single-site
function by the same procedure as in the CPA case, eqns (5.6.10–17).
In this approximation, the final Green function is that given by the MF-
RPA, corresponding to $\Sigma(\mathbf{q}, i\omega_n) = 0$ in (7.2.6). This does not involve
any **q**-summation and may therefore be classified as the $(1/Z)^0$-order re-
sult. In the *cumulant-expansion*, developed by Stinchcombe (1973) and
others, the difference $\mathcal{S}^{(4)} - (\mathcal{S}^{(2)})^2$ is included, to the next order in $1/Z$,
as an additional *vertex* appearing in the interaction chain-diagrams of
$G(\mathbf{q}, i\omega_n)$, independently of the appearance of the $\mathcal{S}^{(2)}$-vertices. A dif-
ferent approach, which is made possible by the isolation of the single-site
Green function in (7.2.5a), is to generalize this equation once more, so
that it becomes a Dyson equation, by replacing $g(i\omega_n)$ with $G(i\omega_n)$ in
the second term on the r.h.s. of (7.2.5a), retaining the correct coefficient
in this term. The effective-medium equation (5.6.13), with $c = 1$, is
valid to first order in $1/Z$, so that

$$G(\mathbf{q}, i\omega_n) = \frac{G(i\omega_n)}{1 + G(i\omega_n)\{\mathcal{J}_{\alpha\alpha}(\mathbf{q}) - K(i\omega_n)\}} \qquad (7.2.7a)$$

and, in combination with the Dyson equation for the single-site Green
function, this leads to a **q**-dependent Green function derived from

$$\Sigma(\mathbf{q}, i\omega_n) = \Sigma(i\omega_n) =$$
$$\frac{1}{n_{01}^2}\Big[(n_0 + n_1 - n_{01}^2)K(i\omega_n) + \frac{1}{\beta g(i\omega_n)} \sum_{n'} g(i\omega_{n'})K(i\omega_{n'})u(n, n')\Big],$$
$$(7.2.7b)$$

where $K(i\omega_n)$ is determined self-consistently, as in (5.6.17),

$$K(i\omega_n) = \sum_{\mathbf{q}} \mathcal{J}_{\alpha\alpha}(\mathbf{q})G(\mathbf{q}, i\omega_n)\Big/ \sum_{\mathbf{q}} G(\mathbf{q}, i\omega_n). \qquad (7.2.7c)$$

The result obtained in this way is close to that derived by Galili and
Zevin (1987) using a more elaborate renormalization procedure, but in
addition to the simplifications attained by utilizing the effective-medium
approximation, the procedure which we have adopted has allowed us to
achieve a fully self-consistent result. We note that, in the application

of the equations of motion, the population factors take the realistic values which may be calculated from eqn (3.5.23) using the more accurate Green functions, whereas the population factors here are by definition the unperturbed MF values. This means that the renormalization of the different RPA parameters predicted by the real part of $\Sigma(\omega)$ includes the possible effects on the population factors. $\Sigma(\omega)$ is the continuation of $\Sigma(i\omega_n)$ on to the real frequency-axis, and the imaginary part of $\Sigma(\omega)$, which is equal to $(n_0 + n_1 - n_{01}^2)/n_{01}^2$ times $\mathrm{Im}\big[K(\omega)\big]$, since the sum in (7.2.7b) is real, predicts a non-zero linewidth for the crystal-field excitations. Introducing the spectral density of the excited states, at positive energies $E = \hbar\omega$,

$$\mathcal{N}(E) = \frac{2}{N} \sum_{\mathbf{q}} \frac{\mathrm{Im}\big[G(\mathbf{q}, E/\hbar)\big]}{\pi E \, G(\mathbf{q}, 0)} \simeq \frac{1}{N} \sum_{\mathbf{q}} \delta(E_{\mathbf{q}} - E),$$

which may be compared with (3.3.17), we find that, at frequencies where $|g(\omega)K(\omega)|$ is small compared to one,

$$\mathrm{Im}\big[K(\omega)\big] \simeq \pi n_{01} M_\alpha^2 \mathcal{N}(\hbar\omega) \Delta / \hbar\omega g^2(\omega),$$

corresponding to a linewidth $2\Gamma_{\mathbf{q}}$ of the excitation at $\mathbf{q}$, half of which is

$$\Gamma_{\mathbf{q}} \simeq \frac{n_0 + n_1 - n_{01}^2}{n_{01}^2} \left(\frac{\Delta^2 - E_{\mathbf{q}}^2}{2E_{\mathbf{q}}} \right)^2 \pi \mathcal{N}(E_{\mathbf{q}}). \qquad (7.2.8a)$$

The linewidth is proportional to the density of states and to the squared energy-difference between the excitation and the crystal-field level (proportional to $\mathcal{J}_{\alpha\alpha}^2(\mathbf{q})$), where the $\mathbf{q}$-dependences of the two factors roughly balance each other. When $E_{\mathbf{q}}$ is close to Δ, this result is no longer valid. Instead, at $\hbar\omega = \widetilde{\Delta}$, where $\widetilde{\Delta}$ is the effective crystal-field splitting determined by $\mathrm{Re}\big[\Sigma(\widetilde{\Delta}/\hbar)\big] = -1/g(\widetilde{\Delta}/\hbar)$, we find that $\mathrm{Re}\big[K(\widetilde{\Delta}/\hbar)\big] = 0$ and

$$\Gamma_{\mathbf{q}}(E_{\mathbf{q}} = \widetilde{\Delta}) \simeq \frac{n_0 + n_1 - n_{01}^2}{n_{01}^2} \frac{1}{\pi \mathcal{N}(\widetilde{\Delta})}. \qquad (7.2.8b)$$

The first result (7.2.8a) for $\Gamma_{\mathbf{q}}$, but not (7.2.8b), agrees with that obtained by the cumulant-expansion method of Stinchcombe (1973) and others. One modification which appears when this method is used is that $K(\omega)$ in (7.2.7b) is replaced by $K(\omega)\{1 - G(\omega)K(\omega)\}$. This is a $(1/Z)^2$-correction, which however becomes important when $\hbar\omega \approx \Delta$, and in this theory $\Gamma_{\mathbf{q}}(E_{\mathbf{q}} = \Delta) = 0$, in contrast to the result (7.2.8b). In order to decide which of the two procedures leads to the most trustworthy results, we have to some extent to rely on the effective-medium

approximation. It is known (Yonezawa 1968) that the cumulant expansion, in solving the dilute RPA equation (5.6.8), includes all terms proportional to $P_2(ij) = \langle c_i c_j \rangle - c^2$, but that this occurs at the expense of 'self-containedness', leading to unphysical features in the final results. Compared to this, the CPA neglects some of the products of $P_2(ii)P_2(jj)$ for neighbouring sites, which are of the order $(1/Z)^2$ (see the discussion following (5.6.17)), but it is self-contained and the results are well-behaved and accurate if Z is not small, as discussed by Elliott *et al.* (1974). Hence, referring to the analyses of the dilute systems, we expect the effective-medium approximation to be more adequate than the unrestricted cumulant expansion in the first order of $1/Z$. More importantly, the Hartree–Fock decoupling of the higher-order cumulants, i.e. $\mathcal{S}^{(6)} = (\mathcal{S}^{(2)})^3 + 3\mathcal{S}^{(2)}\{\mathcal{S}^{(4)} - (\mathcal{S}^{(2)})^2\}$ to first order in $1/Z$, which is one of the basic ideas behind the cumulant-expansion method considered here, does not appear to be a good approximation. The effective-medium model is not solved 'exactly', as this would require a determination of the whole series for $G(i\omega_n)$ in (7.2.5a), but a consideration of the second- and higher-order diagrams in this series indicates that the Dyson-equation generalization is much more reasonable. The sum rules, like (3.3.18) or the 'monotopic restriction' discussed by Haley and Erdös (1972), are satisfied to the considered order in $1/Z$. This is obviously true for the unrestricted cumulant expansion, but it also holds for the effective-medium approximation, as this is derived directly from the behaviour of the single sites. One may ask (Galili and Zevin 1987) whether there exists any other 'conservation law' which permits a more stringent distinction between the various possibilities. For this purpose, we propose to use the condition that the resultant Green function should be independent of adding the following constant to the Hamiltonian:

$$\Delta\mathcal{H} = -\lambda \sum_i \mathbf{J}_i \cdot \mathbf{J}_i = -N\,\lambda J(J+1), \tag{7.2.9}$$

corresponding to a replacement of $\mathcal{J}(\mathbf{q})$ by $\mathcal{J}(\mathbf{q}) + \lambda$. This change does not affect the effective-medium equation (5.6.9), other than by adding the constant to $\mathcal{J}(\mathbf{q})$, so $K(i\omega_n)$ is still determined by (7.2.7c), with λ added on the r.h.s. A replacement of $K(i\omega_n)$ by $K(i\omega_n) + \lambda$ in (7.2.5a) does not make any difference, as $(1/\beta)\sum_{n'} g(i\omega_n')u(n,n') = -g(i\omega_n)$ when $n_0 + n_1 = 1$, so that $J_{i\alpha}J_{i\alpha}$ is a constant. The additions of λ to both $J(\mathbf{q})$ and $K(i\omega_n)$ cancel out in the $\mathbf{q}$-dependent Green function expressed in terms of the single-site Green function, as may be seen from (7.2.7a), so that the final result is independent of λ. This is not the case when the unrestricted cumulant expansion is used. Formally, the occurrence of λ is a $(1/Z)^2$-effect, but this is an unphysical feature which is a serious defect, since λ may assume an arbitrary value. This

variational test is related to the sum rules (like that considered in eqn
(4.2.7) or below), but it has the advantage that it applies directly to the
$\mathbf{q}$-dependent Green function without involving any additional summa-
tions with respect to $\mathbf{q}$ or ω_n. For a final comparison of the two meth-
ods, we may utilize the fact that the single-site series can be summed
exactly in an Ising system with no crystal-field splitting. The result
is $G(\omega) = -\beta\delta_{\omega 0}\langle J_\alpha^2 \exp\{\frac{1}{2}\beta K(0)J_\alpha^2\}\rangle_0 / \langle\exp\{\frac{1}{2}\beta K(0)J_\alpha^2\}\rangle_0$, which co-
incides with that deduced by Lines (1974b, 1975) from his *correlated*
effective-field theory. When $J = 1/2$, the above method produces the
correct result $G(0) = g(0) = -\beta/4$. For the $(J = 1)$-Ising model,
$G(0) = -2\beta[2 + \exp\{-\frac{1}{2}\beta K(0)\}]^{-1}$, which may be compared with the
prediction $G(0) = -2\beta[3 - \frac{1}{2}\beta K(0)]^{-1}$ of eqns (7.2.5–7). On the other
hand, the unrestricted cumulant expansion, to first order in $1/Z$, leads
to spurious contributions of second and higher powers in $K(0)$ and, for
instance, suggests a second-order term in the denominator of $G(0)$ which
is a factor of 14 larger than the correct value. We note that corrections
to the effective-medium theory only appear in the order $(1/Z)^3$ in the
single-site Green function. This comparison is discussed in more detail
by Jensen (1984), in a paper where the $1/Z$-expansion, in the effective-
medium approximation, is combined with the CPA, thereby removing
some of the difficulties encountered in the RPA and mentioned at the
end of Section 5.6.

In a crystal-field system, the single-site fluctuations lead to a non-
zero linewidth of the excitations, to first order in $1/Z$. This reflects the
relative importance of corrections to the RPA, compared to spin-wave
systems. In the latter, the excitation operators are, to a good approxi-
mation, Bose operators, neglecting the 'kinematic' effects, which means
that a non-zero linewidth only appears in the second-order of $1/Z$. The
linewidth $2\Gamma_{\mathbf{q}}$ derived above is exponentially small at low temperatures,
but becomes important when $k_B T \approx \Delta$. The linewidth as a function
of ω, $\Gamma_{\mathbf{q}}(\omega) \propto \mathrm{Im}[K(\omega)]$, is only non-zero as long as $\hbar\omega$ lies within the
excitation energy-band, which roughly corresponds to that determined
by the RPA. This means that the linewidth, in this approximation, be-
gins to decrease at higher temperatures when the RPA-excitation band
becomes sufficiently narrow. The behaviour in both limits is modified
by higher-order effects. Within the framework of the $1/Z$-expansion,
the effective-medium approximation ceases to be valid in second order.
The leading-order scattering effects are due to the single-site fluctuations
and, if the interactions are long-range, the correlation of the fluctuations
on neighbouring sites only leads to minor modifications (provided that
the system is not close to a second-order phase transition). In this kind
of system, the effective-medium method should be satisfactory, and in
order to avoid the complications encountered in more elaborate theo-

ries, we confine ourselves to the $(1/Z)^2$-corrections which can be determined within this approximation. This provides a better estimate of the effects due to the single-site fluctuations, but neglects the possible $\mathbf{q}$-dependence of the self-energy. The correct $(1/Z)^2$-terms in the effective-medium theory are obtained by introducing $\mathcal{S}^{(6)}$ in the third term of the single-site series in eqn (7.2.5). This calculation has been carried out by Jensen *et al.* (1987) for the $(J = 1)$-singlet–doublet case, and the most important effect of the second-order terms is to replace the MF population-factors in (7.2.7b) by approximately the actual population of the excitonic states. Furthermore, $\Gamma_{\mathbf{q}}(\omega)$ becomes non-zero outside the excitation band, and it stays non-zero (although small) in the $T = 0$ limit.

The $(J = 1)$-case has been analysed by Yang and Wang (1975), to first order in $1/Z$, and Bak (1975) independently derived the linewidth and applied the result to Pr. Psaltakis and Cottam (1982) have considered the $(J = 1)$-model in the ordered phase, in the presence of uniaxial anisotropy, where the 'kinematic' effects cannot be neglected. In the paramagnetic singlet–doublet XY-model, the $(1/Z)$-results are close to those derived above for the Ising model. If the xx- and yy-couplings are assumed to be equal, it is found, to a good approximation, that $n_0 + n_1$ in eqn (7.2.7b) is replaced by $n_0 + 2n_1 = 1$, and that the frequency sum in this equation is multiplied by a factor $3/2$. If $\mathcal{J}_{zz}(\mathbf{q})$ is non-zero, it gives rise to additional contributions to the average $\mathbf{q}$-independent self-energy. Furthermore, it also leads to a $\mathbf{q}$-dependent contribution, even in the first order of $1/Z$. This occurs because the odd-rank cumulants (corresponding to half-integral p in (7.2.4)) involving all three components may be non-zero. The lowest-rank odd cumulant which is non-zero is $\langle T_\tau J_{ix}(\tau_1) J_{iy}(\tau_2) J_{iz}(\tau_3)\rangle_0$. Although this formally leads to a $(1/Z)$-contribution to the $\mathbf{q}$-dependent part of $\Sigma(\mathbf{q}, \omega)$, which is not immediately compatible with the effective-medium results above, this should be a minor term in systems with long-range interactions and, if Δ is positive, its importance is much reduced at low temperatures under all circumstances.

The results of calculations of the lifetimes of the long-wavelength magnetic optical-modes in Pr, based on eqn (7.2.7), are compared with the experimental results of Houmann *et al.* (1979) in Fig. 7.4. This theory predicts very nearly the same temperature dependence of the energies as does the self-consistent RPA; the excitation depicted in Fig. 7.4 is the uppermost mode in Fig. 7.3. The theory to first order in $1/Z$ accounts very well for the temperature dependence of the energies, lifetimes, and intensities of these excitations, without adjustable parameters. The low temperature results are similar to those of Bak (1975), but the experiments at the highest temperatures in Fig. 7.4 are more
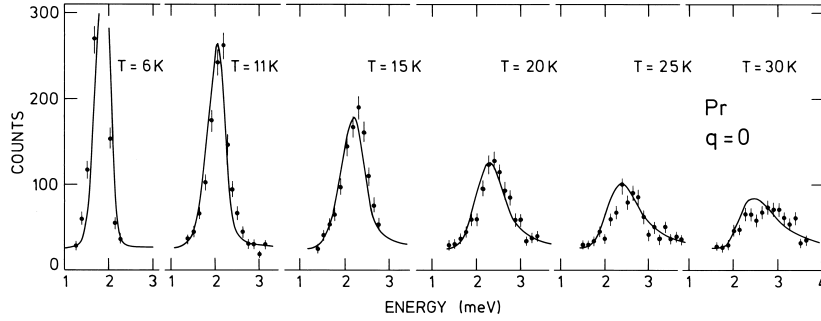
Fig. 7.4. The temperature dependence of the neutron-scattering intensities for the $\mathbf{q} = 0$ magnetic optical-mode on the hexagonal sites of Pr. The instrumental resolution and the overall scaling of the intensity are extracted from the experimental results at 6 K, and thereafter used unchanged in the calculations, which are based on a $1/Z$-expansion, as described in the text.

accurately described by the effective-medium theory developed above, than by his unrestricted cumulant expansion.

An analysis of the $1/Z$-corrections to the MF-RPA theory for the singlet–triplet model does not exist in the literature, to our knowledge. We shall not attempt such an analysis here, but we will discuss one aspect, that the elastic response due to the triplet states is predicted to be a diffusive peak of non-zero width, to first order in $1/Z$, within the effective-medium approximation. In order to consider this matter, we can omit the singlet and use instead the $(J = 1)$ Heisenberg model, corresponding to the above model with $\Delta = 0$. In this case, the diagonal components of the single-site Green function are

$$G(i\omega_n) = -\frac{2}{3}\beta\big\{1 - \tfrac{1}{6}\beta K(0)\big\}\delta_{n0} + \frac{4}{3(i\hbar\omega_n)^2}\big\{K(0) - K(i\omega_n)\big\} + \cdots$$
$$(7.2.10)$$

to first order in $1/Z$. In zero order, the response is purely elastic and $K(i\omega_n) \propto \delta_{n0}$. If this is introduced into (7.2.10), the second term predicts an inelastic contribution to $G(\omega)$, which further diverges proportionally to ω^{-2} in the zero-frequency limit. This divergence indicates that the elastic peak must broaden out to a Lorentzian, with a non-zero half-width Γ, as in (3.3.10–11), corresponding to the replacement of $(\hbar\omega)^2$ in the denominator by $(\hbar\omega)^2 + \Gamma^2$, when the higher-order terms in the series are included. The classification of $K(i\omega_n \neq 0)$ as a higher-order term in the series (7.2.9) is not consistent with a simple Lorentzian,

and a more appropriate form turns out to be

$$G(\omega) = G(0)\left(\frac{i\Gamma}{\hbar\omega + i\Gamma}\right)^2 = G(0)\frac{\Gamma^2\left[\Gamma^2 - (\hbar\omega)^2 + 2i\hbar\omega\Gamma\right]}{\left[\Gamma^2 + (\hbar\omega)^2\right]^2}. \quad (7.2.11a)$$

The real and imaginary parts of this retarded Green function are connected by the Kramers–Kronig relation, and the expansion in powers of Γ agrees with (7.2.10), when

$$G(0) = -\frac{2}{3}\beta\left\{1 - \tfrac{1}{6}\beta K(0)\right\} \qquad \text{and} \quad \Gamma = \sqrt{2K(0)/\beta}. \qquad (7.2.11b)$$

In the high-temperature limit, $K(0) \simeq (2\beta/3N)\sum_{\mathbf{q}} \mathcal{J}^2(\mathbf{q})$, and hence Γ is independent of T in this limit. The most important reason for choosing the Green function given by (7.2.11a) is that it satisfies the sum rule:

$$-\frac{1}{\beta}\sum_{n}\sum_{\alpha=x,y,z} G(i\omega_n) = -3\frac{1}{\pi}\int_0^\infty d(\hbar\omega)\,\mathrm{Im}\big[G(\omega)\big]\coth\left(\beta\hbar\omega/2\right)$$

$$= J(J+1) = 2, \qquad (7.2.12)$$

to the degree of accuracy with which G(0) is determined (this is the same sum rule considered in (4.2.7)). The original expansion series satisfies this sum rule, to first order in $1/Z$, but this property is not easily conserved if a Lorentzian is chosen. The problem with the Lorentzian (with approximately the same Γ as above) is that it decreases only slowly with ω, and the tails lead to a divergence of the integral in (7.2.12), unless a high-frequency cut-off is introduced. In this system, there is no natural frequency-scale setting such a cut-off, and the only reasonable way of determining it is through the sum-rule itself, which is rather unsatisfactory.

In addition to the equations of motion and the Feynman–Dyson linked-cluster-expansion method discussed here, there are other many-body perturbation techniques which may be useful for analysing this kind of system. The most important supplementary theories are those based on the Mori technique (Mori 1965; Huber 1978; Ohnari 1980), or similar projection-operator methods (Becker *et al.* 1977; Micnas and Kishore 1981). However, no matter which theory is used, it cannot circumvent the essential complication of crystal-field systems; the more single-ion levels which are important, the greater is the complexity of the dynamical behaviour. This principle is illustrated by the fact that the methods discussed above have not yet been extended to systems with more than two levels, singlet or degenerate, per site.

7.3 Perturbations of the crystal-field system

In this section, we shall discuss various effects of the surrounding medium on a crystal-field system. The first subject to be considered is the magnetoelastic coupling to the lattice. Its contribution to the magnetic-excitation energies may be described in terms of frequency-dependent, anisotropic two-ion interactions, and we include a short account of the general effect of such terms. We next consider the coupling to the conduction electrons, which is treated in a manner which is very parallel to that used for spin-wave systems in Section 5.7. Finally, we discuss the hyperfine interaction between the angular momenta and the nuclear spins, which becomes important at the lowest temperatures, where it may induce an ordering of the moments in an otherwise undercritical singlet-ground-state system.

7.3.1 Magnetoelastic effects and two-ion anisotropy

The magnetoelastic interactions which, in the kind of system we are considering, primarily originate in the variation of the crystal-field parameters with lattice strain, produce a number of observable phenomena. The lattice parameters and the elastic constants depend on temperature and magnetic field, the crystal-field excitation energies are modified, and these excitations are coupled to the phonons. In addition, the magneto-elastic coupling allows an externally applied uniaxial strain to modify the crystal-field energies. All these magnetoelastic effects have their parallel in the ferromagnetic system discussed in Section 5.4 and, in the RPA, they may be derived by almost the same procedure as that presented there, provided that the spin-wave operators are replaced by the standard-basis operators, introduced in eqn (3.5.11).

In the paramagnetic phase in zero external field, only those strains which preserve the symmetry, i.e. the α-strains, may exhibit variations with temperature due to the magnetic coupling. The lowering of the symmetry by an applied external field may possibly introduce non-zero strains, proportional to the field, which change the symmetry of the lattice. In both circumstances, the equilibrium strains may be calculated straightforwardly within the MF approximation. As an example, we shall consider the lowest-order magnetoelastic γ-strain Hamiltonian

$$\mathcal{H}_\gamma = \sum_i \left[\tfrac{1}{2} c_\gamma (\epsilon_{\gamma 1}^2 + \epsilon_{\gamma 2}^2) - B_{\gamma 2} \{ O_2^2(\mathbf{J}_i)\epsilon_{\gamma 1} + O_2^{-2}(\mathbf{J}_i)\epsilon_{\gamma 2} \} \right], \quad (7.3.1)$$

corresponding to eqn (5.4.1) with $B_{\gamma 4} = 0$. The equilibrium strain $\overline{\epsilon}_{\gamma 1}$, for instance, is determined in the presence of an external magnetic field

and external stresses by

$$\frac{1}{N}\left\langle\frac{\partial \mathcal{H}_\gamma}{\partial \epsilon_{\gamma 1}}\right\rangle = c_\gamma \bar{\epsilon}_{\gamma 1} - B_{\gamma 2}\langle O_2^2\rangle - (t_{11} - t_{22}) = 0,$$

with $\bar{\bar{t}} = (V/N)\bar{\bar{T}}$, where $\bar{\bar{T}}$ is the usual stress-tensor. Introducing the equilibrium condition into the Hamiltonian, we get

$$\mathcal{H}_\gamma(\text{sta}) = -\sum_i B_{\gamma 2}\big\{O_2^2(\mathbf{J}_i)\bar{\epsilon}_{\gamma 1} + O_2^{-2}(\mathbf{J}_i)\bar{\epsilon}_{\gamma 2}\big\} + \mathcal{H}_\gamma^0, \qquad (7.3.2a)$$

where

$$\mathcal{H}_\gamma^0 = N\big[\tfrac{1}{2}c_\gamma(\bar{\epsilon}_{\gamma 1}^2 + \bar{\epsilon}_{\gamma 2}^2) - (t_{11} - t_{22})\bar{\epsilon}_{\gamma 1} - 2t_{12}\bar{\epsilon}_{\gamma 2}\big]. \qquad (7.3.2b)$$

The thermal averages have to be calculated self-consistently, which implies that the static magnetoelastic Hamiltonian, (7.3.2), must itself be included in the total magnetic MF Hamiltonian, which determines the thermal averages such as $\langle O_2^2\rangle$ in the equilibrium equation. The magnetoelastic coupling changes the magnetic-excitation energies if the crystal is strained, because the extra crystal-field term in (7.3.2a), introduced by $\mathcal{H}_\gamma(\text{sta})$, directly modifies $\bar{\bar{\chi}}^o(\omega)$. In the $(J = 1)$-model corresponding to Pr, $O_2^{\pm 2}(\mathbf{J}_i)$ couples the two doublet states, and thus the degeneracy of this level is lifted in proportion to the γ-strains.

Having included the contributions of $\mathcal{H}_\gamma(\text{sta})$ to the single-ion susceptibility, we continue by discussing the influence of the coupling between the magnetic excitations and the phonons, as determined by the dynamic part of the magnetoelastic Hamiltonian $\mathcal{H}_\gamma(\text{dyn})$, given by eqn (5.4.6) with $B_{\gamma 4} = 0$. As an example, we consider the coupling to the transverse phonons propagating in the a- or the b-direction, with the polarization vector in the basal-plane, which is derived from

$$\Delta\mathcal{H}_\gamma(\text{dyn}) = -B_{\gamma 2}\sum_i\big\{O_2^{-2}(\mathbf{J}_i) - \langle O_2^{-2}\rangle\big\}\epsilon_i$$

$$= -B_{\gamma 2}\sum_i\sum_{\nu\mu}N_{\nu\mu}a_{\nu\mu}(i)\epsilon_i, \qquad (7.3.3)$$

where ϵ_i is a shorthand notation for $\epsilon_{\gamma 2}(i) - \bar{\epsilon}_{\gamma 2}$, and $N_{\nu\mu}$ is the matrix element of the Stevens operator between $<\nu|$ and $|\mu>$, cf. eqns (3.5.11–13). This Hamiltonian introduces an additional term on the l.h.s. of the equation of motion (3.5.15) for the Green function $\langle\langle a_{\nu\mu}(i)\,;\,a_{rs}(i')\rangle\rangle$:

$$B_{\gamma 2}\sum_\xi\langle\langle\big\{N_{\mu\xi}a_{\nu\xi}(i) - N_{\xi\nu}a_{\xi\mu}(i)\big\}\epsilon_i\,;\,a_{rs}(i')\rangle\rangle \simeq$$

$$B_{\gamma 2}(n_\nu - n_\mu)N_{\mu\nu}\langle\langle\epsilon_i\,;\,a_{rs}(i')\rangle\rangle, \qquad (7.3.4)$$

where the approximate result follows from the usual RPA decoupling introduced by eqn (3.5.16). According to eqn (5.4.25),

$$\epsilon_i = \sum_{\mathbf{k}} (ikF_{\mathbf{k}}/2)(\beta_{\mathbf{k}} + \beta^+_{-\mathbf{k}})\exp(i\mathbf{k}\cdot\mathbf{R}_i),$$

where we assume, for simplicity, only one phonon mode. From the equations of motion determining the two Green functions $\langle\langle\beta_{\mathbf{q}}\,;\,a_{rs}(i')\rangle\rangle$ and $\langle\langle\beta^+_{-\mathbf{q}}\,;\,a_{rs}(i')\rangle\rangle$, we obtain

$$\langle\langle\beta_{\mathbf{q}} + \beta^+_{-\mathbf{q}}\,;\,a_{rs}(i')\rangle\rangle =$$
$$B_{\gamma 2}\sum_i\sum_{\nu\mu}(iqF_{\mathbf{q}}/2)D(\mathbf{q},\omega)e^{-i\mathbf{q}\cdot\mathbf{R}_i}N_{\nu\mu}\langle\langle a_{\nu\mu}(i)\,;\,a_{rs}(i')\rangle\rangle, \quad (7.3.5)$$

where $D(\mathbf{q},\omega)$ is the phonon Green function for the mode considered:

$$D_\nu(\mathbf{q},\omega) = \frac{2\omega_{\nu\mathbf{q}}}{\hbar(\omega^2 - \omega^2_{\nu\mathbf{q}})}. \quad (7.3.6)$$

If this is introduced into (7.3.4), and the resulting expression is added to the l.h.s. of (3.5.18), the procedure leading to eqn (3.5.21) yields the equivalent result

$$\overline{\overline{\chi}}(\mathbf{q},\omega) - \overline{\overline{\chi}}^o(\omega)\overline{\overline{\mathcal{J}}}(\mathbf{q},\omega)\overline{\overline{\chi}}(\mathbf{q},\omega) = \overline{\overline{\chi}}^o(\omega). \quad (7.3.7)$$

However, these quantities are now four-dimensional matrices in the vector space defined by the operators J_{ix}, J_{iy}, J_{iz}, and $O_2^{-2}(\mathbf{J}_i)$, or more accurately by these operators minus their expectation values. The only extra element in $\overline{\overline{\mathcal{J}}}(\mathbf{q},\omega)$, in addition to the normal Cartesian components $\mathcal{J}_{\alpha\beta}(\mathbf{q})$, is

$$\mathcal{J}_{44}(\mathbf{q},\omega) = N\big(\tfrac{i}{2}qF_{\mathbf{q}}B_{\gamma 2}\big)^2 D(\mathbf{q},\omega). \quad (7.3.8)$$

The excitation energies are determined by the condition

$$\big|1 - \overline{\overline{\chi}}^o(\omega)\overline{\overline{\mathcal{J}}}(\mathbf{q},\omega)\big| = 0.$$

When $\mathbf{q}$ is along an a- or b-direction, and the external fields are applied in the basal plane, parallel or perpendicular to $\mathbf{q}$, then $\overline{\overline{\mathcal{J}}}(\mathbf{q})$ and the 3×3 Cartesian components of $\overline{\overline{\chi}}^o(\omega)$, at low frequencies, are diagonal with respect to the $(\xi\eta\zeta)$-axes. In this case, the most phonon-like pole is found at a frequency determined by

$$\big|1 - \overline{\overline{\chi}}^o(\omega)\overline{\overline{\mathcal{J}}}(\mathbf{q},\omega)\big|\Big/\prod_\alpha\big[1 - \chi^o_{\alpha\alpha}(\omega)\mathcal{J}_{\alpha\alpha}(\mathbf{q})\big] = 1 - \Xi(\mathbf{q},\omega)\mathcal{J}_{44}(\mathbf{q},\omega) = 0,$$
$$(7.3.9a)$$

where $\alpha = \xi$, η, and ζ, and

$$\Xi(\mathbf{q},\omega) = \chi_{44}^o(\omega) + \sum_\alpha \frac{\chi_{\alpha 4}^o(\omega)\chi_{4\alpha}^o(\omega)\mathcal{J}_{\alpha\alpha}(\mathbf{q})}{1 - \chi_{\alpha\alpha}^o(\omega)\mathcal{J}_{\alpha\alpha}(\mathbf{q})}. \qquad (7.3.9b)$$

At long wavelengths, this pole determines the velocity of the magneto-acoustic sound waves, as measured in an ultrasonic experiment, and expressing this velocity in terms of the corresponding elastic constant, we find

$$\frac{c_{66}^*}{c_{66}} = 1 - \Xi(\mathbf{q},0)B_{\gamma 2}^2/c_\gamma, \qquad (7.3.10)$$

by combining the above relation with eqns (5.4.24b) and (5.4.34). This result is valid when $\mathbf{q}$ is along the ξ- or η-axes, provided that the external field is applied along one of the principal axes. In the general case, it is necessary to include the coupling to the other phonon branches in eqn (7.3.7), and also to take into account possible off-diagonal terms in the Cartesian part of the matrices, but these complications may be included in the above calculations in a straightforward fashion. One question raised by (7.3.10) is whether the magneto-acoustic sound velocities, measured at non-zero frequencies, depend on possible purely-elastic contributions to the RPA susceptibilities. That these should be included in (7.3.7), at $\omega = 0$, can be seen by the argument used in deriving (3.5.22). In the preceding section, we found that the coupling between the angular momenta broadens the elastic RPA response into a diffusive peak of width 2Γ, as in (7.2.11b), proportional to $T^{1/2}$ at low temperatures. Unless this coupling is very weak, Γ is likely to be much larger than the applied $\hbar\omega$ in an ultrasonic experiment, in which case the total elastic contribution to $\Xi(\mathbf{q},0)$ in (7.3.10) should be included. A more detailed investigation of this question is given by, for instance, Elliott *et al.* (1972), in a paper discussing systems with Jahn–Teller-induced phase transitions.

In the paramagnetic phase without any external *magnetic* field, the susceptibility components $\chi_{\alpha 4}^o(\omega)$ all vanish in the zero frequency limit, due to the time-reversal symmetry of the system. Replacing t by $-t$ generates the transformation $\chi_{\alpha 4}^o(\omega) \to \chi_{\alpha^T 4^T}^o(-\omega)$, where the time-reversed operators are $J_{i\alpha}^T = -J_{i\alpha}$, and $O_2^{-2}(\mathbf{J}_i)^T = O_2^{-2}(\mathbf{J}_i)$. These results follows from the symmetry properties of the axial tensor operators, discussed after eqn (5.5.14), recalling that the operators are Hermitian, of rank $l = 1$ and $l = 2$ respectively. Hence, because of the time-reversal symmetry, $\chi_{\alpha 4}^o(\omega) = -\chi_{\alpha 4}^o(-\omega) = -\left(\chi_{\alpha 4}^o(\omega^*)\right)^*$, where the last result follows from (3.2.15), and we assume implicitly that all poles lie on the real axis. This quantity must therefore vanish at zero frequency, and the reactive and absorptive components are either zero or purely imaginary at non-zero frequencies. If there is no ordered moment and no

external magnetic field, the coupling between the dipolar crystal-field excitations and the long-wavelength phonons must therefore vanish by symmetry, within the present approximation, and $\Xi(\mathbf{q},0) = \chi^o_{44}(0)$ in eqn (7.3.10). In the presence of an external magnetic field, the mixed dipolar–quadrupolar susceptibility-components may become non-zero, and hence produce a direct coupling of the elastic waves and the dipolar excitations. In this case, the magnetic dipole coupling, which gives rise to a directional dependence of $\mathcal{J}_{\alpha\alpha}(\mathbf{q})$, as discussed in Section 5.5, leads to different values of c^*_{66} (as determined from the transverse sound velocity in the $b(\eta)$-direction), depending on whether the field is parallel to the ξ- or the η-axis or, if the field is fixed along one of these two axes, whether $\mathbf{q}$ is along the ξ- or the η-direction. As mentioned earlier, this anisotropy is similar to that introduced by rotational invariance, and has a comparable magnitude in paramagnetic systems (Jensen 1988b).

The dynamic coupling between the magnetic and elastic excitations in Pr has been studied in the long-wavelength limit by Palmer and Jensen (1978), who measured the elastic constant c_{66} by ultrasonic means, as a function of temperature and magnetic field. At 4 K, it was found to be very sensitive to a field applied in the basal plane, but insensitive to a field along the c-axis, reflecting the anisotropy of the susceptibility. At non-zero fields in the basal plane, there is furthermore a considerable anisotropy, due to B^6_6. Using the crystal-field level scheme illustrated in Fig. 1.16, and a value of $B_{\gamma 2}$ consistent with that deduced from the field dependence of the magnetic excitations (Houmann *et al.* 1979), they were able to obtain a very good fit to the observed dependence of c_{66} on field, shown in Fig. 7.5, and on temperature.

The above theory is also valid at non-zero frequencies. However, if q is no longer small, we must take account of the discreteness of the lattice and replace q in (7.3.8) by a sinusoidal function of q and the lattice parameters, as in (5.4.43) in Section 5.4. Except for the change in the $\mathbf{q}$-dependence of $\mathcal{J}_{44}(\mathbf{q},\omega)$, eqn (7.3.7) still applies, and it predicts hybridization effects between the phonons and the crystal-field excitations, equivalent to those derived from the linear magnon–phonon coupling in Section 5.4. The time-reversal symmetry of the paramagnetic system in zero magnetic field does not exclude the possibility that the phonons at non-zero frequencies are coupled to the crystal-field dipolar excitations and, in the case of Pr, the doublet excitations are allowed to interact with the transverse phonons, when $\mathbf{q}$ is in the c-direction. Nevertheless, the application of a magnetic field will generally introduce new interactions via $\chi^o_{4\alpha}(\omega)$, leading to hybridization effects proportional to the field, as observed in Pr by Houmann *et al.* (1979) and interpreted by Jensen (1976a). Interactions between crystal-field excitations and
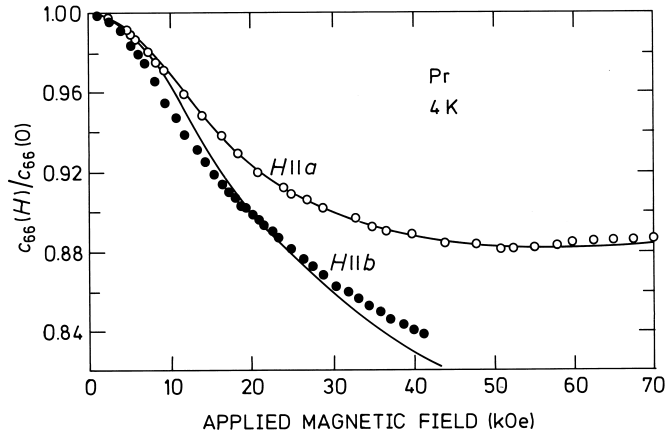
Fig. 7.5.   The field dependence of the elastic constant c_{66} in Pr at 4 K, relative to the value at zero field. The elastic constant was determined from the velocity of the transverse sound waves propagating in an a-direction, and the open and closed symbols indicate the experimental results when the field was applied respectively in the a- or the perpendicular b-direction. The solid lines show the calculated field dependence.

the phonons are further discussed by Thalmeier and Fulde (1975), Fulde (1979), and Aksenov *et al.* (1981).

The coupling (5.4.50), quadratic in the magnon operators, also has its counterpart in crystal-field systems. Such interactions arise when, instead of applying the RPA decoupling in the first step, as in eqn (7.3.4), we proceed to the next step in the hierarchy of Green functions. The most important effect of these terms is to replace the crystal-field parameters by effective values, which might be somewhat temperature dependent, corresponding to an averaging of the effective crystalline field experienced by the 4f electrons over the finite volume spanned by the thermal vibration of the ions. As in the spin-wave case, these extra higher-order contributions do not lead to the kind of hybridization effects produced by the linear couplings. However, if the density of states of the phonons, weighted with the amplitude of the coupling to the crystal-field excitations, is particularly large at certain energies, resonance-like bound-states due to the higher-order terms may be observed in the magnetic spectrum. The *dynamic Jahn–Teller effect* observed in CeAl$_2$ (Loewenhaupt *et al.* 1979) seems to be due to these higher-order effects, according to the calculation of Thalmeier and Fulde (1982).

The expression (7.3.7) for the interaction of the crystal-field system with the phonons has essentially the same form as that derived from any

general two-ion coupling. Referring to (5.5.14), in which is introduced a general two-ion Hamiltonian in terms of the tensor operators $\widetilde{O}_{lm}(\mathbf{J}_i)$, we may write

$$\mathcal{H}_{\mathrm{JJ}} = -\frac{1}{2} \sum_{ij} \mathbf{J}_i^p \cdot \overline{\overline{\mathcal{J}}}^p(ij) \cdot \mathbf{J}_j^p, \tag{7.3.11}$$

where $\mathbf{J}^p \equiv (J_x, J_y, J_z, O_2^{-2}, \widetilde{O}_{lm}, \cdots)$ is a generalized p-dimensional moment operator, and the $\{lm\}$-set of operators comprises the tensor couplings from the original Hamiltonian, except those between the first four components. It is then immediately clear that the final RPA susceptibility is given by an expression equivalent to (7.3.7), in terms of the $p \times p$ susceptibility-matrix with $\mathcal{J}_{\alpha\beta}(\mathbf{q},\omega) = \mathcal{J}_{\alpha\beta}^p(\mathbf{q})$, except that (at long wavelengths) $\mathcal{J}_{44}(\mathbf{q},\omega) = N(iqF_{\mathbf{q}}B_{\gamma2}/2)^2 D(\mathbf{q},\omega) + \mathcal{J}_{44}^p(\mathbf{q})$. If the frequency is not near a pole in $D(\mathbf{q},\omega)$, the effect of the coupling to the phonons on the magnetic excitations is therefore similar to that stemming from the corresponding quadrupole–quadrupole interaction. If $\mathcal{J}_{44}^p(\mathbf{0})$ is non-zero, the ultrasonic velocities are influenced by this coupling, as we now have

$$\frac{c_{66}^*}{c_{66}} = \frac{1 - \Xi(\mathbf{q},0)\mathcal{J}_{44}(\mathbf{0},0)}{1 - \Xi(\mathbf{q},0)\mathcal{J}_{44}^p(\mathbf{0})} = 1 - \frac{\Xi(\mathbf{q},0)}{1 - \Xi(\mathbf{q},0)\mathcal{J}_{44}^p(\mathbf{0})} B_{\gamma2}^2/c_\gamma, \tag{7.3.12}$$

where the sum over α in (7.3.9b) comprises all the $(p-1)$ components for which $\alpha \neq 4$, under the same condition that $\overline{\overline{\chi}}^o(\omega)$ and $\overline{\overline{\mathcal{J}}}(\mathbf{q},\omega)$ are both diagonal for $\alpha \neq 4$. In general, $\chi_{4\alpha}^o(0)$ may be non-zero, in the paramagnetic phase in zero magnetic field, if the α-component is an even-rank tensor, and these interactions may contribute to $\Xi(\mathbf{q},0)$, whereas the odd-rank couplings are prevented from affecting the phonons in the zero-frequency limit by time-reversal symmetry.

In our discussion of crystal-field excitations, we have only been concerned with the excitation spectrum derived from the time variation of the *dipole* moments. There are two reasons for this. Most importantly, the coupling between the dipolar moments expressed in eqn (7.1.1) is normally dominant in rare earth systems, so that the collective phenomena are dominated by the dipolar excitations. The other reason is that the *magnetic* response, including the magnetic susceptibility and the (magnetic) neutron scattering cross-section, is determined exclusively by the upper-left 3×3 part of $\overline{\overline{\chi}}(\mathbf{q},\omega)$, in the generalized p-dimensional vector space introduced through eqn (7.3.11). However, strong quadrupolar interactions may lead to collective effects and to an ordered phase of the quadrupole moments. The quadrupolar excitations are not directly visible in neutron-scattering experiments, but may be detected indirectly via their hybridization with the dipole excitations, in the same way as the phonons, or via their hybridization with the phonons, as measured

by the nuclear scattering of the neutrons. In a paramagnetic system in zero field, the $p \times p$ susceptibility-matrix partitions into two independent blocks, at zero frequency, the one depending only on the even-rank couplings and the other only on the odd-rank couplings. If one of the two parts of $\overline{\overline{\chi}}(\mathbf{q}, 0)$ diverges at some temperature T^*, it signals the occurrence of a second-order phase transition at this temperature. If it is the block determined by the even-rank couplings which diverges, the order parameter below T^* is associated with the quadrupole moments, assuming the lowest-rank terms to be dominant. If there is any coupling between this order parameter and one of the phonon modes, the transition is accompanied by a softening of these phonons, provided that the pure quadrupolar excitations have higher energies than the phonons at the ordering wave-vector. If this vector $\mathbf{Q}$ is zero, the corresponding elastic constant vanishes at the transition. In the case where $\mathbf{Q} \neq \mathbf{0}$, the situation corresponds to that considered in the magnetic case, and the phonon mode shows soft-mode behaviour according as there are pure elastic contributions to the (RPA) susceptibility or not. A quadrupolar phase-transition involving the phonons is usually referred to as being induced by the *Jahn–Teller* effect, and a more detailed discussion and relevant examples may be found in, for instance, Elliott *et al.* (1972). The presence of a non-zero quadrupole moment does not destroy the time-reversal symmetry, and an ordering of the dipole moments may follow only after an additional phase transition. In TmZn (Morin *et al.* 1980) an ordering of the quadrupole moments occurs below a first-order transition at $T_Q = 8.6\,\mathrm{K}$, and this phase is disrupted by the onset of ferromagnetic ordering at $T_C = 8.1\,\mathrm{K}$. In the opposite case of ordering of the dipole moments, the breaking of the time-reversal symmetry allows a direct coupling between the dipole and quadrupole moments, so that the latter are forced to order together with the dipoles, giving rise to, for example, crystal-field-induced magnetostriction effects, and the dipolar ordering will normally quench any tendency toward a purely quadrupolar-ordered phase.

In this chapter, we have formulated the various RPA results in terms of the generalized-susceptibility matrices. The results apply in paramagnetic as well as in ordered systems, so long as the order parameter is uniform throughout the crystal. They agree with the more explicit results derived previously in the case of a weakly-anisotropic ferromagnetic system. In a paramagnet or a strongly-anisotropic ferromagnet, the results above may also be given a more transparent and explicit form, but only if the number $(2J + 1)$ of different angular-momentum states can be taken as small; else the matrix-equations themselves are well-suited for solution by numerical methods. The reduction of the matrix-equations in, for instance, the $(J = 1)$-case is straightforward

and the results, corresponding to Pr in the limit $T = 0$, are given by Jensen (1976a).

In the present approximation, the sound velocities are not affected by the interaction between the dipoles, in the paramagnetic phase at zero magnetic field. However, in the vicinity of a second-order transition to a ferromagnetic phase, strong softening of the long-wavelength phonons may be observed, depending on the symmetry properties, and this behaviour cannot be explained within the RPA. We have seen that, according to eqns (5.4.15) and (5.4.38), c_{66}^* vanishes in the basal-plane ferromagnet when a field equal to the critical field H_c is applied along the hard basal-plane direction. When T_C is approached from below, H_c vanishes rapidly, resulting in a strong softening of c_{66}^* even in zero field, and it seems likely that similar behaviour should be observed when T_C is approached from above, considering that just above T_C there will be large domains of nearly constant magnetization, allowing an 'RPA' coupling between the dipole moments and the sound waves similar to that occurring in the ferromagnetic phase. Clear indications of this kind of behaviour have been seen in for example Tb (Jensen 1971b), indicating that the RPA is not even qualitatively trustworthy when the fluctuations are a dominating feature of the system.

7.3.2 Conduction-electron interactions

The *sf*-exchange Hamiltonian (5.7.6) was derived without making any special assumptions about the rare earth metal involved, and it therefore applies equally well to a metallic crystal-field system. For the weakly-anisotropic ferromagnet considered in Section 5.7, this Hamiltonian leads to a Heisenberg two-ion coupling, $\widetilde{\mathcal{J}}(\mathbf{q}, \omega)$, which to a first approximation is instantaneous, and is thus effectively $\mathcal{J}(\mathbf{q}) = \widetilde{\mathcal{J}}(\mathbf{q}, 0) - (1/N) \sum_{q'} \widetilde{\mathcal{J}}(\mathbf{q}', 0)$, as given by eqn (5.7.28). This remains true in crystal-field systems, as may be demonstrated by expanding the angular-momentum operators in (5.7.6) in terms of the standard-basis operators, and then calculating the corresponding Green functions which determine $\overline{\overline{\chi}}(\mathbf{q}, \omega)$, utilizing an RPA decoupling of the coupled Green functions.

In the ordered phase, $\mathcal{J}_{zz}(\mathbf{q}, \omega)$ may actually differ from the two other components of the exchange coupling, due to the polarization of the conduction electrons. However, in the paramagnetic phase in zero field, the coupling is isotropic, within the approximation made in Section 5.7. This may be seen by analysing the full expression (5.7.27) for $\widetilde{\mathcal{J}}(\mathbf{q}, \omega)$, or the simpler result (5.7.26), in which the susceptibility of the conduction electrons becomes a scalar:

$$\chi_{\text{c.el.}}^{\alpha\beta}(\mathbf{q}, \omega) = \tfrac{1}{2}\chi_{\text{c.el.}}^{+-}(\mathbf{q}, \omega)\, \delta_{\alpha\beta}. \qquad (7.3.13)$$

Here the reactive and absorptive parts of $\chi_{\text{c.el.}}^{+-}(\mathbf{q},\omega)$, still given by (5.7.26$b$), are both real and even in $\mathbf{q}$, while the reactive part is even with respect to ω, whereas the absorptive part is odd. When considering the frequency dependence of the susceptibility, we must distinguish two separate regimes, defined by the parameter

$$\vartheta = -\eta q/2k_F = (\hbar\omega/2\varepsilon_F)(k_F/q) = (2/3\nu)\mathcal{N}(\varepsilon_F)\hbar\omega(k_F/q),$$

where η is the parameter introduced in (5.7.31c) (with $\Delta(\text{c.el.}) = 0$). If $|\vartheta|$ is small compared to one,

$$\chi_{\text{c.el.}}^{+-}(\mathbf{q},\omega) = \mathcal{N}(\varepsilon_F)\left\{\mathcal{F}\left(\frac{q}{2k_F}\right) + i\frac{\pi}{2}\vartheta\right\} \qquad ; \quad |\vartheta| \ll 1, \qquad (7.3.14)$$

where the correction to the real part, of the order ϑ^2, may be neglected. This is the same result as obtained in the ordered phase, eqns (5.7.32) and (5.7.36), when the small frequency-dependent term in the former is neglected. When $|\vartheta|$ becomes larger than 1 (or $q > 2k_F$), the imaginary part vanishes, as shown in the calculations leading to (5.7.36), and the real part becomes strongly dependent on ω, vanishing for large values of ϑ as $\vartheta^{-2} \propto \omega^{-2}$. If $\hbar\omega = 1\text{--}10\,\text{meV}$, then $\vartheta = (10^{-4} - 10^{-3})k_F/q$ in the rare earth metals, so that the corrections to (7.3.14) are only important in the immediate neighbourhood of $q = 0$. The physical origin of this particular effect is that the susceptibility of the free-electron gas is purely elastic in the limit $q = 0$, and it does not therefore respond to a uniform magnetic field varying with a non-zero frequency. In the polarized case, the contributions to the transverse susceptibility are all inelastic at long wavelengths, so this retardation effect does not occur when the polarization gap $\Delta(\text{c.el.})$ is large compared to $|\hbar\omega|$. The exchange coupling, in the limit $q = 0$, includes both the elastic and inelastic contributions, as in (5.7.26c), and the abnormal behaviour of the elastic term may be observable in paramagnetic microwave-resonance experiments, where the anomalies should be quenched by a magnetic field. On the other hand, it may not be possible to study such an isolated feature in $\mathbf{q}$-space by inelastic neutron-scattering experiments. Leaving aside the small-q regime, we have therefore that the effective exchange-coupling is

$$\mathcal{J}(\mathbf{q},\omega) = \mathcal{J}(\mathbf{q}) + i\zeta(\mathbf{q})\hbar\omega, \qquad (7.3.15)$$

where $\zeta(\mathbf{q})$ is given by (5.7.37b), and $\mathcal{J}(\mathbf{q})$ is the reduced zero-frequency coupling given above, or by (5.7.28).

In the case of the weakly-anisotropic ferromagnet, the frequency dependence of the exchange coupling affects the spin-wave excitations

in the same way as results when $\mathcal{J}(\mathbf{q})$ is replaced by $\mathcal{J}(\mathbf{q}, \omega)$ in the usual RPA expression for the susceptibility, i.e.

$$\overline{\overline{\chi}}(\mathbf{q}, \omega) = \left\{ 1 - \overline{\overline{\chi}}^o(\omega) \mathcal{J}(\mathbf{q}, \omega) \right\}^{-1} \overline{\overline{\chi}}^o(\omega). \qquad (7.3.16)$$

In order to establish that this procedure is valid in general, to leading order in $1/Z$, we must appeal to the $1/Z$-expansion discussed in Section 7.2. It is clear that the usual RPA decoupling (3.5.16), $a_{\nu\xi}(i)a_{\nu'\mu'}(j) \simeq \langle a_{\nu\xi}(i) \rangle a_{\nu'\mu'}(j) + a_{\nu\xi}(i) \langle a_{\nu'\mu'}(j) \rangle$, is not a good approximation if $i = j$, and in (3.5.15) it is only applied in cases where $i \neq j$, as $\mathcal{J}(ii) = 0$ by definition. Here, however, $\mathcal{J}(\mathbf{q}, \omega)$ does contain a coupling of one ion with itself, since $\mathcal{J}(ii, \omega) = i\zeta_0 \hbar \omega$, where

$$\zeta_0 = \frac{1}{N} \sum_{\mathbf{q}} \zeta(\mathbf{q}) = 2\pi \langle |j(\mathbf{q})|^2 \rangle \mathcal{N}^2(\varepsilon_F), \qquad (7.3.17)$$

as is obtained by replacing $|j(\mathbf{q})|$ in (5.7.37b) by a constant averaged value in the integral determining ζ_0. This indicates that it is also necessary to rely on the RPA decoupling when $i = j$, in order to obtain the result (7.3.16) when ζ_0 is not zero. On the other hand, the RPA decoupling may work just as well if only the time arguments of the two operators are different, which is the case as $\mathcal{J}(ii, t = 0) = 0$ independently of ζ_0. Only when $t = 0$, is $a_{\nu\xi}(i, t)a_{\nu'\mu'}(i, 0)$ equal to $a_{\nu\mu'}(i, 0)\delta_{\xi\nu'}$, in direct conflict with the RPA decoupling. This indicates that it may not be necessary to consider separately the effects of $\zeta(\mathbf{q}) - \zeta_0$ and of ζ_0. This point is treated more precisely by the $1/Z$-expansion procedure developed in Section 7.2. Since $\mathcal{J}(\mathbf{q}, \omega)$ replaces $\mathcal{J}(\mathbf{q})$, it makes no difference whether $\mathcal{J}(\mathbf{q}, \omega)$ is frequency-dependent or not, nor whether $\mathcal{J}(ii, \omega) \neq 0$, and this procedure leads immediately to the result (7.3.16), in the zeroth order of $1/Z$. If $\mathcal{J}(\mathbf{q}, \omega)$ contains a constant term, resulting from $\mathcal{J}(ii, t) \propto \delta(t)$, it is removed automatically in the next order in $1/Z$, according to the discussion following eqn (7.2.9). The argument for subtracting explicitly any constant contribution to $\mathcal{J}(\mathbf{q}, \omega)$, in eqn (7.3.16), is then that this procedure minimizes the importance of the $1/Z$ and higher-order contributions. The modifications of the $1/Z$ contributions are readily obtained by substituting $\mathcal{J}(\mathbf{q}, \omega)$ for $\mathcal{J}(\mathbf{q})$ in the expression (7.2.7c), which determines $K(\omega)$, i.e.

$$\widetilde{K}(\omega) = K(\omega) + \frac{1}{N} \sum_{\mathbf{q}} i\zeta(\mathbf{q}) \hbar \omega G(\mathbf{q}, \omega)/G(\omega) = K(\omega) + i\langle \zeta(\omega) \rangle \hbar \omega,$$

$$(7.3.18a)$$

and the self-energy is then obtained as

$$\Sigma(\mathbf{q}, \omega) = i\zeta(\mathbf{q}) \hbar \omega + \widetilde{\Sigma}(\omega), \qquad (7.3.18b)$$

where $\widetilde{\Sigma}(\omega)$ is the previous function with $K(\omega)$ replaced by $\widetilde{K}(\omega)$. The most interesting effects of the scattering of the magnetic excitations against the electron-hole pair excitations of the conduction electrons derive from the first term in the self-energy, which already appears in the 'RPA' in (7.3.16). The lifetime of the excitations becomes $\mathbf{q}$-dependent and remains finite in the zero-temperature limit, whereas the imaginary part of $\Sigma(\omega)$, and therefore also of $\widetilde{\Sigma}(\omega)$, vanishes exponentially at low temperatures, in the order $1/Z$. The importance of the higher-order contributions associated with this scattering mechanism, as compared to those of the intrinsic processes, i.e. the relative magnitudes of $\langle\zeta(\omega)\rangle\hbar\omega$ and $K(\omega)$, may depend on the system considered, but in Pr, for example, $\text{Im}\big[K(\omega)\big]$ is much the dominant term at frequencies lying within the excitonic band. Hence, $\langle\zeta(\omega)\rangle$ may be neglected in $\widetilde{K}(\omega)$ at temperatures where the linewidths are still somewhat smaller than the overall bandwidth.

In Pr, the effect of the conduction electrons on the linewidths at low temperatures only becomes visible due to the strong increase in the value of $\zeta(\mathbf{q})$ in the limit of small q, where it is approximately proportional to $1/q$. Houmann et $al.$ (1979) were thus able to observe the remarkable broadening of the acoustic modes illustrated in Fig. 7.6, as q was reduced at $6\,\text{K}$. The width at $q = 0.2\,\text{Å}$ is only slightly greater than the experimental resolution, but the peak has become very broad by $0.05\,\text{Å}$, and it has almost vanished into the background at $q = 0$, even though the integrated intensity is expected to increase as the energy decreases. This behaviour is in sharp contrast to that observed in Tb where, as shown in Fig. 5.13 on page 269, the width at small q is greatly reduced by the spin-splitting of the Fermi surface, in accordance with eqn (5.7.37). Since the spin-splitting of the Pr Fermi surface becomes very substantial in a large field, as illustrated in Fig. 1.10, the scattering of the long-wavelength magnetic excitations by the conduction electrons should be quenched by the application of a field. A careful study of this phenomenon would allow a detailed investigation of the interaction between the conduction electrons and the $4f$ moments.

The modification of $\widetilde{K}(\omega)$ also contributes to the broadening of the diffusive peak and, instead of (7.2.11), the result for $J = 1$ is now

$$G(\omega) = G(0)\frac{i\Gamma_1\hbar\omega - \Gamma^2}{(\hbar\omega + i\Gamma)^2}, \qquad (7.3.19a)$$

with

$$\Gamma_1 = 2\langle\zeta(0)\rangle/\beta \qquad \text{and} \quad \Gamma = \Gamma_1 + \sqrt{2K(0)/\beta}. \qquad (7.3.19b)$$

The term linear in $\langle\zeta(0)\rangle$, introduced in (7.2.10), predicts Lorentzian broadening, if $K(0)$ is neglected. The intrinsic contribution may also
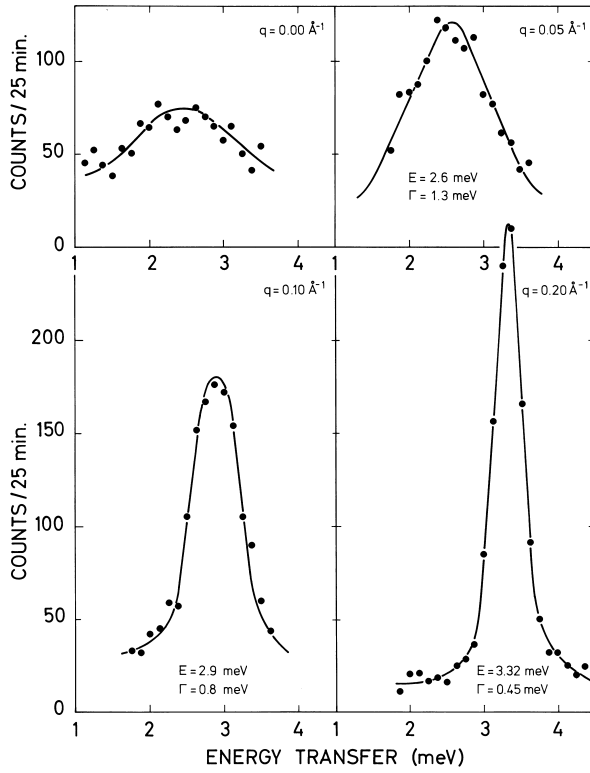
Fig. 7.6.   Neutron-scattering spectra from the acoustic branch of the magnetic excitations propagating along the c-axis on the hexagonal sites of Pr at 6 K. The observed values of Γ, the full width at half maximum, increase rapidly as q decreases, due to scattering by the conduction electrons, and at $q = 0$ it is difficult to distinguish the peak from the background. The experimental energy resolution is about 0.35 meV.

here dominate at most temperatures, but it is clear that this cannot hold true in the high-temperature limit, where Γ_1 increases proportionally to T, whereas $K(0)/\beta$ approaches a constant value. So, in the high-temperature limit, (7.3.19) leads to the *Korringa law* (Korringa 1950) for the linewidth:

$$G(\mathbf{q}, \omega) \simeq G(\omega) \simeq G(0) \frac{i\Gamma_1}{\hbar\omega + i\Gamma_1}, \qquad \text{with}$$

$$\Gamma_1 = 2\langle \zeta(0) \rangle k_B T = 4\pi \langle |j(\mathbf{q})|^2 \rangle \mathcal{N}^2(\varepsilon_F) k_B T, \qquad (7.3.20)$$

since $\langle \zeta(0) \rangle = \zeta_0$ in this limit. We argued above that $\langle \zeta(\omega) \rangle$ could be neglected, in comparison with the intrinsic effects, at relatively low

temperatures but, in the high-temperature limit, $\langle \zeta(\omega) \rangle$ is the dominant term. Becker *et al.* (1977) have deduced the influence of the electron-hole-pair scattering on the crystal-field excitations, with an accuracy which corresponds to the results obtained here to first order in $1/Z$, using an operator-projection technique. They performed their calculations for an arbitrary value of J, but without including the intrinsic damping effects which, as pointed out above, may be more important, except in the high-temperature limit.

The effects of the *sf*-exchange Hamiltonian on the effective mass and the heat capacity of the conduction electrons in a crystal-field system may be derived in an equivalent way to that used for the spin-wave system. The mass-enhancement, $m^*/m = 1 + \lambda_{\mathrm{CF}}$, is deduced to be given by (White and Fulde 1981; Fulde and Jensen 1983):

$$
\begin{aligned}
\lambda_{\mathrm{CF}} &= \mathcal{N}(\varepsilon_F) \frac{1}{2k_F^2} \int_0^{2k_F} dq \int \frac{d\Omega_{\mathbf{q}}}{4\pi} q |j(\mathbf{q})|^2 \sum_\alpha \chi_{\alpha\alpha}(\mathbf{q}, \omega \to 0) \\
&= \frac{1}{N} \sum_{\mathbf{q}} \frac{\zeta(\mathbf{q})}{2\pi \mathcal{N}(\varepsilon_F)} \sum_\alpha \chi_{\alpha\alpha}(\mathbf{q}, \omega \to 0),
\end{aligned}
$$

$$(7.3.21a)$$

and is a generalization of eqn (5.7.50), valid in the paramagnetic phase. The term $\chi_{\alpha\alpha}(\mathbf{q}, \omega \to 0)$ is the zero-frequency susceptibility, omitting possible elastic contributions, assuming the broadening effects to be small. At non-zero temperatures, it is found that excitations with energies small compared to $k_B T$ do not contribute to the mass-enhancement, and therefore, even in the low-temperature limit considered here, the purely elastic terms in $\chi_{\alpha\alpha}(\mathbf{q}, \omega)$ do not influence the effective mass. This is also one of the arguments which justifies the neglect to leading order of the effect on m^* of the longitudinal fluctuations in a ferromagnet, which appear in $\chi_{zz}(\mathbf{q}, \omega)$. In contrast, the elastic part of the susceptibility should be included in eqn (5.7.57), when the magnetic effects on the resistivity are derived in the general case, as in Section 5.7. In systems like Pr, with long-range interactions, the dispersive effects due to the $\mathbf{q}$-dependence of $\overline{\overline{\chi}}(\mathbf{q}, \omega)$ are essentially averaged out, when summed over $\mathbf{q}$. In this case, we may, to a good approximation, replace $\overline{\overline{\chi}}(\mathbf{q}, \omega)$ in sums over $\mathbf{q}$ by its MF value $\overline{\overline{\chi}}^o(\omega)$. The correction to the MF value of the low-temperature heat capacity in Pr, for example, is minute (Jensen 1982b). In the eqns (7.3.18–20) above, this means that, to a good approximation, $\langle \zeta(\omega) \rangle \simeq \frac{1}{N} \sum_{\mathbf{q}} \zeta(\mathbf{q}) = \zeta_0$ even at low temperatures, and that the mass-enhancement parameter is

$$
\lambda_{\mathrm{CF}} \simeq \frac{\zeta_0}{2\pi \mathcal{N}(\varepsilon_F)} \sum_\alpha \chi_{\alpha\alpha}^o(\omega \to 0). \qquad (7.3.21b)
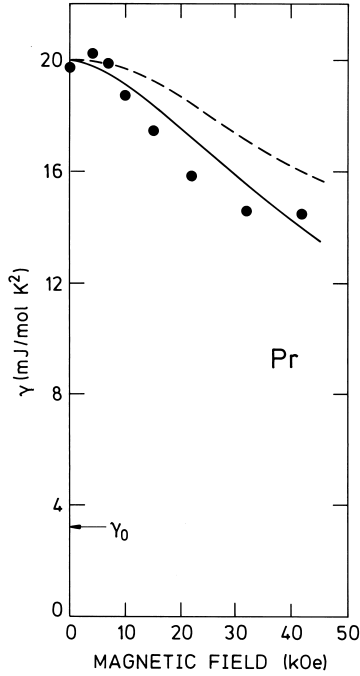$$

Fig. 7.7. The field dependence of the coefficient γ of the linear electronic heat capacity of Pr at low temperatures. The experimental results of Forgan (1981) are compared with a theory including the renormalization of the mass, due to the interaction of the conduction electrons with the magnetic excitations, and also taking into account the phonon enhancement and the dependence of the Fermi level on magnetic field. The dashed line shows the results of the theory when the change of the Fermi energy with field is neglected.

The mass-enhancement due to the crystal-field excitations is reflected directly in the effective mass measured in the de Haas–van Alphen effect, and in the linear term in the low-temperature electronic specific heat, analogously to the spin-wave system. The former effect has been studied by Wulff *et al.* (1988), who find that the theory of Fulde and Jensen (1983) accounts very well for the field dependence of the masses of several orbits, using the same values of the sf-exchange integral I, about $0.1\,\mathrm{eV}$, as reproduce the variation of the orbit areas discussed in Section 1.3. The substantial field dependence of the electronic heat capacity, measured by Forgan (1981), is shown in Fig. 7.7, and compared with values calculated from eqn (7.3.21b), taking into account the field dependence of the electronic state density at the Fermi level, calculated by Skriver (private communication), and the phonon enhancement (Skriver and Mertig 1990). At higher temperatures, the imaginary part of $\mathcal{J}(\mathbf{q}, \omega)$ in (7.3.16) gives rise to the same contribution to the magnetic heat capacity as the extra term in (5.7.52) in the spin-wave case, with $\zeta(\mathbf{q}) \sum_\alpha \chi_{\alpha\alpha}(\mathbf{q}, \omega \to 0)$ replacing $2\Gamma_{\mathbf{q}}/E_{\mathbf{q}}^2$. This contribution should be added to the non-linear corrections to the total low-temperature heat capacity calculated by Fulde and Jensen (1983).

7.3.3 Coupling to the nuclear spins

The hyperfine coupling to the nuclear spins normally has a negligible influence on the properties of the electronic magnetic moments. However, in the special case of a crystal-field system with a singlet ground-state, where the two-ion coupling is smaller than the threshold value for magnetic ordering, this minute coupling may become of decisive importance. Under these circumstances, the hyperfine interaction may induce a cooperative ordering of the combined system of the electronic and nuclear magnetic moments at very low temperatures. The Hamiltonian describing the hyperfine interaction in a rare earth ion has been comprehensively discussed by Bleaney (1972) and McCausland and Mackenzie (1979), and the leading-order term is

$$\mathcal{H}_{\mathrm{hf}} = A\,\mathbf{I}\cdot\mathbf{J}, \tag{7.3.22}$$

where $\mathbf{I}$ is the nuclear spin. For the isotope of Pr with mass number 141, which has a natural abundance of 100%, $I = 5/2$ and $A = 52.5\,\mathrm{mK} = 4.5$ μeV. This coupling modifies the MF susceptibility $\overline{\overline{\chi}}^{o}(\omega)$ of the single ion, and since A is small, we may derive this modification by second-order perturbation theory. In order to simplify the calculations, we assume that the MF ground-state of the electronic system is a singlet, and that $k_B T$ is much smaller than the energy of the lowest excited J-state, so that any occupation of the higher-lying J-states can be neglected. Considering first a singlet–singlet system, with a splitting between the two states $|0>$ and $|1>$ of $\Delta \gg |A|$, where only $M_z = <0|\,J_z\,|1>$ is non-zero, and denoting the combined electronic and nuclear states by $|0, m_I>$ and $|1, m_I>$, where $I_z|p, m_I> = m_I|p, m_I>$, we find that the only non-zero matrix elements of $\mathcal{H}_{\mathrm{hf}}$ are

$$<0, m_I|\,\mathcal{H}_{\mathrm{hf}}\,|1, m_I> = <1, m_I|\,\mathcal{H}_{\mathrm{hf}}\,|0, m_I> = m_I M_z A,$$

yielding the following modifications of the state vectors:

$$\begin{cases} |0', m_I> = |0, m_I> -(m_I M_z A/\Delta)|1, m_I> \\ |1', m_I> = |1, m_I> +(m_I M_z A/\Delta)|0, m_I>, \end{cases}$$

to leading order. If we neglect the shifts in energy of the different levels, due to the hyperfine coupling, and the change of the inelastic matrix element,

$$<0', m_I|\,J_z\,|1', m_I> = M_z\{1 - (m_I M_z A/\Delta)^2\} \simeq M_z,$$

the susceptibility is only modified by the non-zero matrix-element,

$$<0', m_I|\,J_z\,|0', m_I> = -2m_I M_z^2 A/\Delta,$$

within the $(2I + 1)$-ground state manifold, i.e.

$$\delta\chi_{zz}^{o}(\omega) = \beta\frac{1}{2I+1}\sum_{m_I}\left(2m_I M_z^2 A/\Delta\right)^2\delta_{\omega 0} = \beta\frac{1}{3}I(I+1)A^2(2M_z^2/\Delta)^2\delta_{\omega 0}.$$

(7.3.23)

This result may be straightforwardly generalized to an arbitrary level scheme, including non-zero matrix elements of the other **J**-components, as the different contributions are additive. The susceptibility may then be written

$$\chi_{\alpha\beta}^{o}(\omega) = \chi_{\alpha\beta}^{J}(\omega) + A^2\sum_{\gamma\gamma'}\chi_{\alpha\gamma}^{J}(\omega)\chi_{\gamma\gamma'}^{I}(\omega)\chi_{\gamma'\beta}^{J}(\omega),$$

(7.3.24)

to leading order in A, which is valid as long as the general assumptions made above are satisfied. $\chi_{\alpha\beta}^{J}(\omega)$ is the MF susceptibility for the electronic system alone, when the extra term $\delta\mathcal{H}_J(\text{MF}) = A\langle\mathbf{I}\rangle\cdot\mathbf{J}$ is included in its MF Hamiltonian. In order to derive the effective MF Hamiltonian $\mathcal{H}_I(\text{MF})$, determining the susceptibility of the nuclear spins $\chi_{\alpha\beta}^{I}(\omega)$, we must consider the possibility, neglected above, that $\mathcal{H}_{\text{hf}}$ may lift the $(2I + 1)$-fold degeneracy of the ground-state manifold. Calculating the energies of the ground-state levels, in the presence of an external field, by second-order perturbation theory, we find straightforwardly that the equivalent Hamiltonian, describing the splitting of these levels, is

$$\mathcal{H}_I(\text{MF}) = -g_N\mu_N\mathbf{H}\cdot\mathbf{I} + A\{\langle\mathbf{J}\rangle + A\langle\mathbf{I}\rangle\cdot\overline{\overline{\chi}}^{J}(0)\}\cdot\mathbf{I} - \tfrac{1}{2}A^2\mathbf{I}\cdot\overline{\overline{\chi}}^{J}(0)\cdot\mathbf{I}.$$

(7.3.25a)

This result can be interpreted as expressing the ability of **J** to follow instantaneously any changes of **I**. The molecular field due to $\langle\mathbf{J}\rangle$ is subtracted from the response to **I**, which then instead gives rise to the last quadrupolar term. This quadrupolar contribution is the only effect which is missing in a simple RPA decoupling of the interactions introduced through $\mathcal{H}_{\text{hf}}$. If $\overline{\overline{\chi}}^{J}(0)$ is not a scalar, the last term gives rise to a quadrupole-splitting of the ground-state manifold, and the zero-frequency susceptibility is then, to leading order in this term,

$$\chi_{\alpha\alpha}^{I}(0) = \tfrac{1}{3}I(I+1)\beta\left[1 + \tfrac{1}{15}A^2\beta(I+\tfrac{3}{2})(I-\tfrac{1}{2})\{3\chi_{\alpha\alpha}^{J}(0) - \sum_{\gamma}\chi_{\gamma\gamma}^{J}(0)\}\right]$$

(7.3.25b)

if $\overline{\overline{\chi}}^{J}(0)$ is diagonal. The results above were first obtained and analysed by Murao (1971, 1975, 1979), except that he replaced $\chi_{\alpha\alpha}^{J}(0)$ in (7.3.25) by $(1/N)\sum_{\mathbf{q}}\chi_{\alpha\alpha}^{J}(\mathbf{q},0)$ which, according to the above interpretation, is to be expected in order $1/Z$. For the hexagonal ions in Pr-metal, $A\chi_{\alpha\alpha}^{J}(0) = 0.026$ for the two basal-plane components, but is

zero for the cc-component, which implies that the induced quadrupolar-interaction is a factor of about seven larger than the intrinsic value of the electric-quadrupole hyperfine-interaction for the ion ($< 0 |\, \mathcal{H}_Q \,| 0 > = (5/7)P_\parallel(I_\xi^2 + I_\eta^2)$, with $P_\parallel = -0.128\,\text{mK}$, using the notation of Bleaney (1972)). In any case, the quadrupole contribution to (7.3.25b) only makes a 1.5% correction at the transition temperature $T_N \approx 50\,\text{mK}$ in Pr. The induced quadrupole interaction, due to the highly anisotropic fluctuations of the electronic moments, may be important in nuclear-magnetic-resonance (NMR) experiments. The most important effect in NMR is, however, the strong enhancement of the Zeeman splitting between the nuclear levels by the hyperfine coupling. Introducing $\mathcal{H}_I(\text{MF}) = -g_N\mu_N \mathbf{H}_I^{\text{eff}} \cdot \mathbf{I}$ in (7.3.25a), we find an enhancement

$$|H_I^{\text{eff}}/H| \simeq |1 - (g\mu_B/g_N\mu_N)A\chi_{zz}(\mathbf{0}, 0)|, \qquad (7.3.26)$$

which, for the hexagonal ions in Pr, gives a factor of about 40 in the low-temperature limit, when the field is applied in the basal-plane, but unity if H is along the c-axis. In addition to the hyperfine interactions considered above, the nuclear spins may also interact directly with the conduction electrons, leading to an extra *Knight shift* and Korringa broadening of the NMR-levels. The most important NMR-linewidth effect is, however, due to the fluctuations of the localized electronic moment. If $J = 1$, corresponding to Pr, these fluctuations lead to a Lorentzian broadening, so that $\chi_{\xi\xi}^I(0) \to \chi_{\xi\xi}^I(0)\big[i\Gamma_N/(\hbar\omega + i\Gamma_N)\big]$, with

$$\Gamma_N = 10(n_0 n_1/n_{01})M_\xi^2 \text{Im}\big[\widetilde{K}(\omega = \Delta/\hbar)\big],$$

to first order in $1/Z$. In the case of Pr, this gives $\Gamma_N \simeq \exp(-\beta\Delta) \times 1.0$ meV (Jensen *et al.* 1987).

The magnetization and the neutron-scattering cross-section are determined in the RPA by the usual susceptibility expression (7.1.2), with $\overline{\overline{\chi}}^o(\omega)$ now given by (7.3.24), provided that we neglect the contributions of the small nuclear moments. This means that, even though the electronic system has a singlet ground-state, the hyperfine interaction induces an elastic contribution, and assuming the electronic system to be undercritical, so that $R(0) < 1$ in (7.1.6), we obtain in the low temperature limit, where $k_B T \ll \Delta$,

$$\chi_{\xi\xi}(\mathbf{q}, 0) = \frac{\Delta^2\big\{1 + A^2\chi^J(0)\chi^I(0)\big\}}{E_{\mathbf{q}}^2 - (\Delta^2 - E_{\mathbf{q}}^2)A^2\chi^J(0)\chi^I(0)}\chi^J(0), \qquad (7.3.27)$$

where $\chi^J(0) = 2M_\xi^2/\Delta$, and $E_{\mathbf{q}}$ is given by (7.1.4b), with $n_{01} = 1$. If we introduce the nuclear spin susceptibility, neglecting the quadrupolar contribution, into this expression, it predicts a second-order phase

transition, at a temperature determined by

$$k_B T_N = \tfrac{1}{3} I(I+1) A^2 \chi^J(0) \frac{\Delta^2 - E_{\mathbf{Q}}^2}{E_{\mathbf{Q}}^2} = \tfrac{1}{3} I(I+1) A^2 \chi^J(0) \frac{R_0}{1-R_0},$$
(7.3.28)

to a modulated phase described by the wave-vector $\mathbf{Q}$ at which $\mathcal{J}(\mathbf{q})$ has its maximum value, where R_0 is the critical parameter defined by eqn (7.1.6). With $\Delta = 3.52\,\mathrm{meV}$ and $E_{\mathbf{Q}} = 1.0\,\mathrm{meV}$ for the hexagonal excitations in Pr, the electronic system is just undercritical, with a critical ratio $R_0 \simeq 0.92$. This means that the importance of the hyperfine interaction is much enhanced, and eqn (7.3.28) predicts $T_N = 45\,\mathrm{mK}$ for the cooperative ordering of the nuclear and electronic moments in Pr. The transition is no longer accompanied by a soft mode, but there is rather an elastic peak, with a scattering intensity given by

$$\mathcal{S}_d^{\xi\xi}(\mathbf{q}, \omega \approx 0) = \tfrac{1}{3} I(I+1) A^2 \frac{(2M_\xi^2/E_{\mathbf{q}})^2}{1 - \chi^J(0)\{1 + A^2 \chi^J(0)\chi^I(0)\}\mathcal{J}(\mathbf{q})} \delta(\hbar\omega),$$
(7.3.29)

in the paramagnetic phase, which diverges at $\mathbf{q} = \mathbf{Q}$ when T approaches T_N, analogously to the behaviour of the singlet–triplet case described by (7.1.13).

7.4 Magnetic properties of Praseodymium

The magnetic behaviour of Pr has already been extensively discussed in this chapter, in order to illustrate a number of the phenomena which occur in crystal-field systems. In this section, we will collect together these threads into a coherent description of the magnetic ordering which may be induced by various perturbations, and of the excitations in the paramagnetic and ordered phases.

7.4.1 Induced magnetic ordering

As discussed at the end of the preceding section, the coupling of the nuclear spins to the electronic moments in Pr gives rise to a magnetic system whose ground state is degenerate. According to the third law of thermodynamics, this degeneracy must be lifted at sufficiently low temperatures and, within the MF approximation, this is accomplished by magnetic ordering at a temperature determined by eqn (7.3.28). The enhancement factor $R_0/(1-R_0)$ is about 12 for the hexagonal sites, so that the calculated collective-ordering temperature for the nuclear spins and the electronic moments is raised into the more readily accessible range of about $45\,\mathrm{mK}$. The strong neutron-diffraction peak illustrated in Fig. 7.8 was observed at $40\,\mathrm{mK}$ by Bjerrum Møller *et al.* (1982), at a value of $\mathbf{Q}$ close to the minimum in the dispersion relations of the magnetic excitons. This mode of excitation comprises magnetic fluctuations

whose zero-frequency limit is a longitudinal-wave structure along the b-axis, and the electronic moment induced by the hyperfine coupling, in the zero-temperature limit, is

$$\langle J_\eta(\mathbf{Q})\rangle_0 \simeq IA\frac{\chi^J(0)}{1 - \chi^J(0)\mathcal{J}(\mathbf{Q})} = IA\frac{2M_\eta^2}{\Delta(1 - R_0)}, \qquad (7.4.1)$$

multiplied by $g\mu_B$, corresponding to about $0.6\,\mu_B$. Determining the electronic moment from the neutron-diffraction intensities is complicated by the coherent nuclear scattering of neutrons at the same $\mathbf{Q}$, due to the induced polarization of the nuclei. The two contributions can however be separated with the help of polarized neutrons, and Kawarazaki *et al.* (1988) thereby deduced that the electronic moment on the hexagonal sites is about $0.4\,\mu_B$ at $30\,\text{mK}$, while there is also an induced moment an order of magnitude smaller on the cubic sites. The nuclear polarization on both types of site is substantial at this temperature, which is consistent with the observation by Lindelof *et al.* (1975) and Eriksen *et al.* (1983) of a dramatic increase in the nuclear heat capacity, indicating a second-order transition of the nuclear spins to an ordered structure at about $50\,\text{mK}$.

As may be seen in Fig. 7.8, the magnetic ordering is preceded by a strong precursor scattering, which has been observed in single crystals by a number of investigators at temperatures as high as $10\,\text{K}$, and was first investigated in the millikelvin range by McEwen and Stirling (1981). The figure shows that the peak actually comprises two contributions, one centred at the critical wave-vector, and a broader component at a slightly smaller wave-vector. The narrower peak, which is usually known as the *satellite*, appears around $5\,\text{K}$ and increases rapidly in intensity as T_N is approached, at which temperature it transforms into the magnetic Bragg peak. Since the width in $\boldsymbol{\kappa}$ of this peak is greater than the instrumental resolution, at temperatures above T_N, it does not reflect the presence of true long-range magnetic order, but rather very intense fluctuations, with a range of several hundred Å, which presumably also vary slowly in time. The RPA theory predicts such a peak only because of the elastic scattering from the nuclear spins, as given by eqn (7.3.29). However, the peak produced by this mechanism is estimated to be visible only very close to T_N, below $200\,\text{mK}$, and cannot therefore explain the observations. The satellite above T_N may be interpreted as a critical phenomenon, due to the strong increase in the fluctuations, neglected in the RPA, which develop as the second-order transition is approached. When the electronic susceptibility has saturated below about $7\,\text{K}$, the critical fluctuations in Pr would be expected
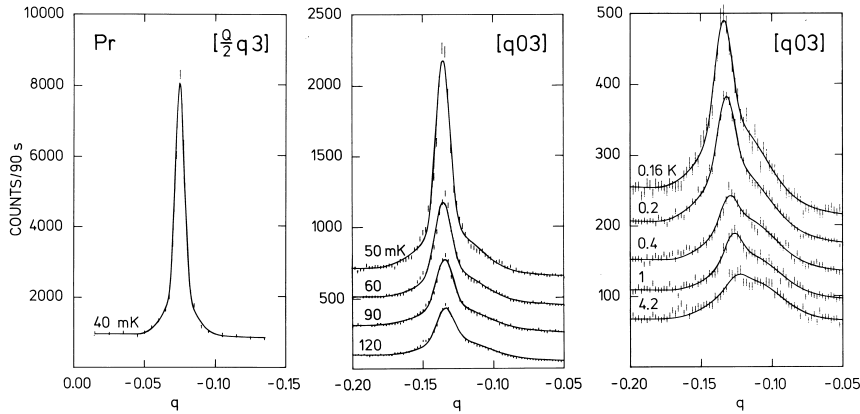
Fig. 7.8.   Neutron-diffraction scans in Pr. The solid lines show the sum of two Gaussian functions fitted to the data. Only below 50 mK is the width of the narrower of these equal to the experimental resolution, indicating true long-range magnetic order.

to correspond to those of a normal degenerate system within 10% of its critical temperature. However, the satellite in Fig. 7.8 is much more intense than such fluctuations could normally give rise to. An alternative possibility, which has been analysed theoretically by Murao (1984), is that much of the intensity of the satellite above T_N is due to an ordering of the moments close to the surface of the crystal, which gives rise to a Bragg peak of non-zero width. The crystalline electric field acting on the surface ions is different from that determining the bulk properties, and the magnetic response of these ions will therefore also be different. For instance, the lowering of the symmetry near the surface splits the degeneracy of the $|\pm 1>$-states, thereby enhancing one of the basal-plane components of the susceptibility tensor.

The occurrence of the other peak in the scans shown in Fig. 7.8, known as the *central* or *quasielastic peak*, has been a long-standing mystery. It is much broader than the satellite and constitutes a ring of scattering around Γ in the basal-ΓMK-plane, with a radius which is slightly smaller than that of the contour of energy mimima found in the excitation spectrum, illustrated in Fig. 7.1. The integrated quasielastic-scattering intensity from this ring is therefore rather large, and around 1 K it is found to correspond to a moment of the order of $0.1\,\mu_B$ per hexagonal ion. In a polycrystalline sample, this ring of scattering cannot be distinguished from scattering from a single point in $\boldsymbol{\kappa}$-space, which presumably explains why diffraction studies of polycrystalline Pr indicate that it is antiferromagnetic at 4 K (Cable *et al.* 1964).

The quasielastic peak cannot be classified as an additional critical phenomenon, because it is not centred at the critical ordering wave-vector. Furthermore, even though its intensity increases in the para-magnetic phase, as the system approaches criticality, it is still present, with a non-zero width in $\boldsymbol{\kappa}$-space, below the transition and its intensity continues to increase as the temperature is further reduced (Burke *et al.* 1981; Bjerrum Møller *et al.* 1982; McEwen 1986). The dynamic effects associated with this quasielastic peak are very modest, as observed by Jensen *et al.* (1987); its width in energy is estimated to be less than 0.1 meV. Nevertheless, its integrated intensity is too large to be explained as a static phenomenon due to scattering from local *short-range* ordering of the crystal near the surface or around bulk defects, such as magnetic impurities or lattice defects. The only remaining possibility appears to be that the quasielastic peak is associated with the magnetic response of the itinerant electrons. This is consistent with one of the results of the neutron-scattering studies by Leuenberger *et al.* (1984) of the hexagonal *insulator* $Cs_3Cr_2Br_9$, in which the Cr dimers form a singlet–triplet system which has a number of analogies to Pr. Even though this system is very close to magnetic ordering, and the lowest excitation energies are only about 0.2 meV, there is no sign of either a satellite or a quasielastic peak. The spin fluctuations of band electrons are not normally expected to give rise to a quasielastic peak of the intensity observed in Pr, and its occurrence may therefore indicate the formation of resonant states near the Fermi surface in Pr, due to hybridization of the conduction electrons with the $4f$ electrons. As discussed in Section 1.3, the $4f$ electrons in Pr are very close to delocalization, and the incipient magnetic instability of the localized electrons would therefore be expected to be reflected in fluctuations in the conduction electron-gas. An indication of the sensitivity of the conduction electrons to the ordering process is provided by the resistivity measurements of Hauschultz *et al.* (1978), who found an increase of almost fifty per cent, over the temperature range in which the quasielastic peak develops, in the c-direction, where superzone effects in the ordered phase are expected to be of minor importance. Further studies of the quasielastic peak, and associated changes in the conduction electrons, particularly under high pressures with the corresponding progressive increase in $4f$ hybridization, would clearly be of interest.

Antiferromagnetism can also be induced in Pr by an internal coupling to magnetic impurities. Assuming that the susceptibility of the single impurities of concentration c is proportional to $1/T$, we find that eqns (5.6.5–6) of the virtual crystal approximation lead to an ordering temperature determined by

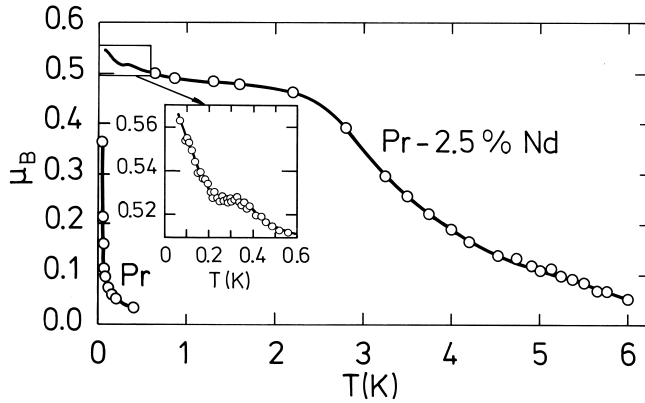$$T_N = T_N(c) = \frac{c}{1 - (1-c)R(T_N)} T_N(c=1), \qquad (7.4.2)$$

Fig. 7.9.   The effective moments, deduced from the intensities of the
narrower peaks in scans of the type illustrated in Fig. 7.8, in Pr and
$Pr_{97.5}Nd_{2.5}$. Only below about $50\,mK$ and $3.5\,K$ respectively do these
moments correspond to a long-range magnetically ordered state.

where $R(T)$ is the critical parameter of eqn. (7.1.6). This expression
gives $T_N \simeq 12.5cT_N(c = 1)$, for $c \ll 1$. A rapid increase of T_N at
small concentrations of Nd ions in Pr was indeed observed by Lebech
et al. (1975). As illustrated in Fig. 7.9, the study of a single crystal of
$Pr_{97.5}Nd_{2.5}$ by Bjerrum Møller *et al.* (1982) revealed a number of infor-
mative details. The temperature dependence of the scattered intensity
follows qualitatively the behaviour observed in pure Pr. The quasielastic
peak appears around $10\,K$, a strong satellite which is broader than the
experimental resolution emerges from it around $6\,K$, and a diffraction
peak, signifying true long-range order, develops below about $3.5\,K$. As
in Pr, the quasielastic peak continues to grow below T_N. The rise in
the magnetization below about $0.2\,K$ is ascribed to the polarization of
the nuclei and their hyperfine interaction with the $4f$ moments. Inelas-
tic neutron-scattering experiments by Wulff *et al.* (1983) gave results
consistent with a crystal-field model in which the Nd ions have a pre-
dominantly $|\pm\frac{3}{2}>$ ground state, and excited $|\pm\frac{1}{2}>$ and predominantly
$|\pm\frac{5}{2}>$ states at about $0.3\,meV$ and $1.2\,meV$ respectively.

The application of an external uniaxial pressure along the a-axis
in the basal plane lifts the degeneracy of the $|\pm 1>$ first excited-state
and may therefore induce magnetic ordering, as predicted by Jensen
(1976a) and observed by McEwen *et al.* (1978). The magnetoelastic
phenomena described in Section 7.3.1, particularly the magnitude of the
field-induced interaction between the magnetic excitations and the trans-
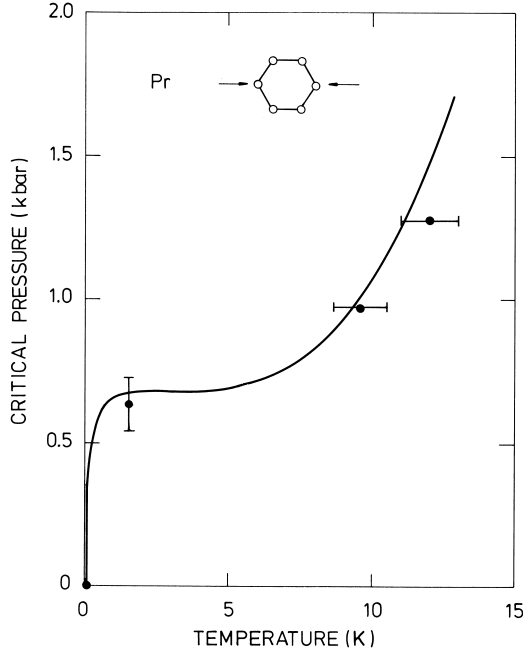verse phonons, may be used for estimating the coupling parameter $B_{\gamma 2}$

Fig. 7.10.   MF calculation of the ordering temperature T_N in Pr, as
a function of the uniaxial pressure in the a-direction, compared with the
neutron-diffraction measurements of McEwen *et al.* (1983).

for the hexagonal ions. Neglecting the magnetoelastic coupling to the
cubic ions, we obtain from eqn (7.3.2) the following γ-strain contribution
to the magnetic Hamiltonian:

$$\mathcal{H}_\gamma(\text{sta}) = -\sum_{i\in\text{hex.ions}} \mathrm{B}_{\gamma 2}\mathrm{O}_2^2(\mathbf{J}_\mathrm{i})\big[\tfrac{1}{2}\mathrm{B}_{\gamma 2}\langle\mathrm{O}_2^2(\mathbf{J}_\mathrm{i})\rangle + \mathrm{t}_{11}\big]/\mathrm{c}_\gamma + \mathcal{H}_\gamma^0,\ \ (7.4.3)$$

in the presence of a uniaxial stress along the ξ-axis. N in (7.3.2) is
the total number of ions, or twice the number of hexagonal sites. At
zero temperature and zero magnetic field, the only effect of $\mathcal{H}_\gamma(\text{sta})$,
within the effective $(J = 1)$-model, is that the crystal-field splitting
which determines the excitation spectrum becomes different for the two
polarizations, and for instance Δ_η, giving the J_η-mode energies, is found
to be

$$\Delta_\eta = \Delta_\eta(t_{11}) = \Delta - B_{\gamma 2}M_{22}t_{11}/c_\gamma,$$
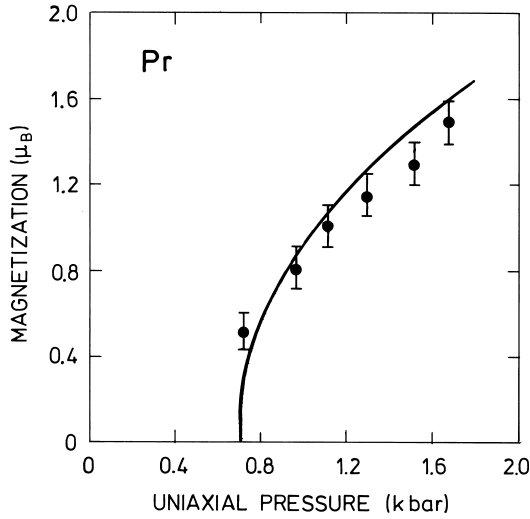
Fig. 7.11.   Experimental measurements of the first harmonic of the magnetization on the hexagonal sites in Pr, deduced from the intensities of neutron-diffraction peaks at $1.5\,\mathrm{K}$, compared with a MF calculation for the $J = 4$ ion.

where the matrix element

$$M_{22} \equiv\; <1_\mathrm{a}|O_2^2|1_\mathrm{a}> = -\,<1_\mathrm{a}|J_\eta^2|1_\mathrm{a}> = -10,$$

in Pr. Δ_ξ differs from Δ by the same amount, but with the opposite sign. At the incipient ordering wave-vector $\mathbf{Q}$ along the η-axis, the excitations are purely transverse or longitudinal, J_ξ or J_η modes. The critical ratio R_0, defined by eqn (7.1.6), for the optical longitudinal mode at $\mathbf{Q}$ is then determined by

$$R_0(t_{11}) = R_0(0)\Delta/\Delta_\eta(t_{11}).$$

Hence the application of the stress alters the critical ratio, and it attains the threshold value 1 when

$$T_{11}^c = \frac{\{1 - R_0(0)\}\Delta}{M_{22}B_{\gamma2}}\,c_\gamma N/V, \qquad (7.4.4)$$

where $c_\gamma N/V = 4c_{66}$. With the following values of the parameters; $R_0(0) = 0.92$, $\Delta = 3.52\,\mathrm{meV}$, $B_{\gamma2} \simeq 12\,\mathrm{meV}$, and $c_{66} = 1.6 \cdot 10^{10}\,\mathrm{N/m^2}$, the effective $(J = 1)$-model predicts that the critical stress necessary for inducing magnetic ordering in Pr at zero temperature is $T_{11}^c = -1.5$ kbar. However, the $|3_\mathrm{s}>$-state lies just above the magnetic excitons
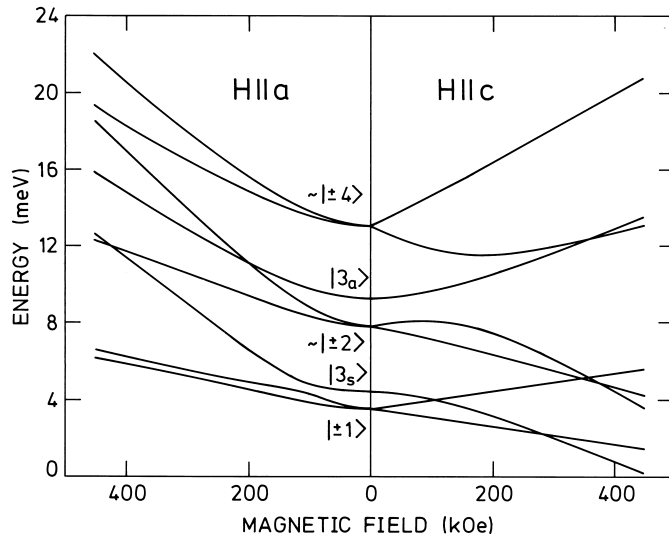
Fig. 7.12.   The crystal-field levels of an isolated hexagonal ion in Pr, as a function of an applied magnetic field in the *a*- and *c*-directions. The zero-field wavefunctions are specified more precisely in Fig. 1.16.

and, as $< 1_\mathrm{a} | O_2^2 | 3_\mathrm{s} >$ is non-zero, it has a significant effect on $\Delta_\eta(t_{11})$. A calculation which includes all the crystal-field levels of Pr predicts the critical uniaxial pressure $-T_{11}^c$ along the ξ-axis to be 0.7 kbar. As may be seen in Fig. 7.10, such a calculation is in good agreement with the experimental observations of McEwen *et al.* (1983), at temperatures sufficiently high that the hyperfine coupling is of no importance, and also accounts very well for the critical pressure at higher temperatures, where the thermal population of the magnetic excitons becomes significant. The dependence of the ordered moment at 1.5 K on the uniaxial pressure is also very well reproduced by this theory, as illustrated in Fig. 7.11. The stable configurations of the moments at zero pressure are expected to be analogous to those found in Nd and discussed in Sections 2.1.6 and 2.3.1, i.e. a single-**Q** structure at small values of the magnetization and a double-**Q** configuration when the first harmonic of the moments is larger than about 0.2–0.3 μ_B. This behaviour has not been established experimentally, but a suggestive rotation of the ordering wave-vector away from the symmetry axis, as expected in the double-**Q** structure, has been detected (McEwen *et al.* 1983). Uniaxial pressure stabilizes a longitudinal wave with **Q** along the *b*-axis perpendicular to the strain, and a modest pressure of about 0.1 kbar is estimated to be sufficient to quench the double-**Q** structure. Accordingly, the theoretical curve in
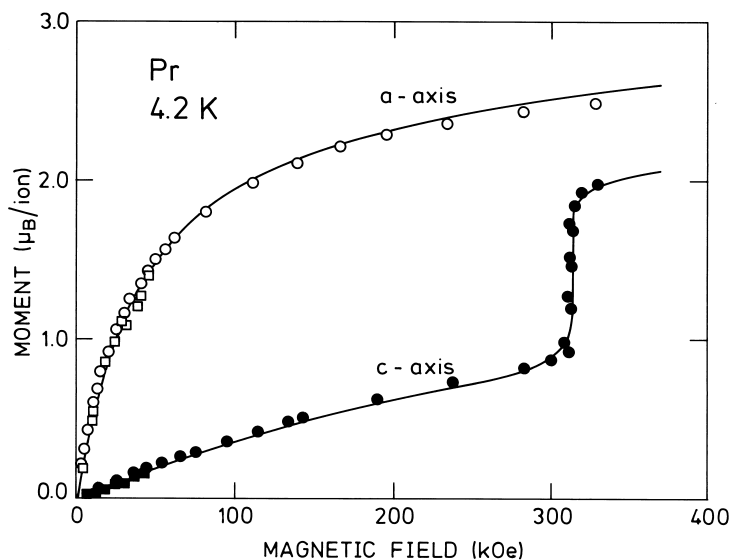
Fig. 7.13.   MF calculation of the magnetization of Pr at 4.2 K as a function of a magnetic field applied in the a- and c-directions. The circles are the experimental measurements of McEwen *et al.* (1973), while the squares are deduced from the neutron-diffraction results of Lebech and Rainford (1971).

Fig. 7.11 is calculated with the assumption of a single-$\mathbf{Q}$ ordering of the moments.

The final perturbation which may induce a magnetic state in Pr is an external magnetic field. The modification of the crystal-field levels of an isolated hexagonal ion by a magnetic field is illustrated in Fig. 7.12. If the field is in the basal plane, the excited states are increased in energy, relative to the ground state, but they mix strongly into it, giving rise to the large moment shown in Fig. 7.13. If the magnetic field is along the c-axis, on the other hand, the matrix elements between the ground and excited states on the hexagonal sites are zero, but the $|+1>$ and $|3_\mathrm{S}> \rightarrow |+3>$ states both decrease in energy, linearly and quadratically respectively. At about 320 kOe, the latter crosses the ground state and the moment increases abruptly, as observed by McEwen *et al.* (1973). As illustrated in Fig. 7.13, the model of Houmann *et al.* (1979), supplemented with a magnetoelastic coupling $B_{\alpha 2} = 7.0$ meV for the hexagonal ions, accounts well for these results. The jump in the magnetization rapidly becomes smeared out when the temperature is raised, due to the thermal population of the excited states, as observed experimentally at 14 K (McEwen 1978).

7.4.2 The magnetic excitations

The magnetic-excitation spectrum in Pr has been investigated experi-
mentally in great detail as a function of various external constraints,
such as the temperature, a magnetic field applied in the basal plane, and
uniaxial pressure. Most of the knowledge about the (low-temperature)
coupling parameters in the model Hamiltonian for Pr, which we have al-
ready utilized several times in the preceding sections, has been derived
from these experiments. The first inelastic neutron-scattering exper-
iments on Pr (Rainford and Houmann 1971; Houmann *et al.* 1975b)
showed that the excitations behave as expected in a singlet ground-
state system, and that the two-ion coupling is just below the threshold
value for inducing magnetic ordering. A MF analysis of the tempera-
ture dependence of the excitations, shown by the dashed lines in Fig.
7.3, indicated that the crystal-field splitting Δ between the $|0>$ ground-
state and the first excited $|\pm 1>$-doublet state of the hexagonal ions is
about 3.2 meV. An important discovery (Houmann *et al.* 1975b) was the
observation, illustrated in Fig. 7.1, of a strong splitting of the doublet
excitations, whenever such a splitting is allowed by symmetry, i.e. when
$\mathbf{q}$ is not along the c-axis. This effect demonstrates that the anisotropic
contribution to the two-ion Hamiltonian of Pr,

$$\mathcal{H}_{\mathrm{JJ}} = -\frac{1}{2} \sum_{ij} \mathcal{J}(ij)\, \mathbf{J}_i \cdot \mathbf{J}_j$$

$$+ \frac{1}{2} \sum_{ij} \mathcal{K}(ij) \big[(J_{i\xi} J_{j\xi} - J_{i\eta} J_{j\eta}) \cos 2\phi_{ij} + (J_{i\xi} J_{j\eta} + J_{i\eta} J_{j\xi}) \sin 2\phi_{ij} \big],$$

$$(7.4.5)$$

is important. Here ϕ_{ij} is the angle between the ξ-axis and the projection
of $\mathbf{R}_i - \mathbf{R}_j$ on the basal plane. Real-space coupling parameters $\mathcal{J}(ij)$
and $\mathcal{K}(ij)$ derived from the excitation energies shown in Fig. 7.1, using
the MF-RPA expression for the energies with $\Delta = 3.52$ meV, are shown
in Fig. 1.18. This somewhat larger value of Δ was obtained from a
study of the field dependence of the excitations (Houmann *et al.* 1979),
but it is still consistent with their temperature dependence, as shown
by the results of the self-consistent RPA, the solid lines in Fig. 7.3.
Besides leading to the more accurate value of Δ, the field experiments
revealed the presence of a rather strong magnetoelastic γ-strain coupling
in Pr, which creates energy gaps proportional to the field at the crossing
points of the magnetic-exciton and transverse-phonon branches in the
basal-plane directions, as illustrated in Fig. 7.14.

The model Hamiltonian, with the two-ion and magnetoelastic terms
given respectively by (7.4.5) and (7.4.3), together with the usual single-
ion crystal-field Hamiltonian for a hexagonal system, describes very well
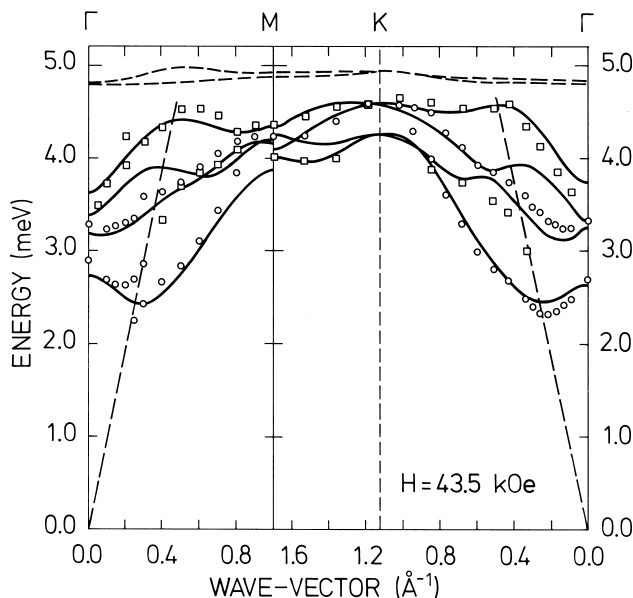the excitation-energy changes observed by Houmann *et al.* (1979) when

Fig. 7.14.   Dispersion relations for the excitations propagating on the hexagonal sites of Pr at 6 K, in an applied field of 43.5 kOe. The field is in the basal plane and perpendicular to the wave-vector, so that there is a discontinuity at M, corresponding to a rotation of the field through 90°. Compared with Fig. 7.1, the energy of the magnetic excitations has increased, and the field has induced couplings between the magnetic excitons and the transverse-acoustic phonons polarized in the basal plane, indicated by dashed lines. These phonons are coupled to the acoustic and optical longitudinal magnetic modes in the ΓM-direction, and to the (predominantly) acoustic longitudinal and optical transverse modes (the two branches of intermediate energy) in the ΓK-direction (Jensen 1976a). The full lines show the results of an RPA calculation of the magnetic excitations, neglecting the coupling to the phonons. The predicted low-intensity higher-lying modes, corresponding to transitions to the predominantly $|3_s>$ crystal-field state, were not observed directly in the experiments, but their influence may be seen in the lowest branch along ΓK, since it is their mixing with this mode which holds the energies below those along ΓM.

a field is applied in the basal plane at low temperature. The dispersion relation was measured at three values of the field (14.5, 29.0, and 43.5 kOe), and the results obtained at the highest field are shown in Fig. 7.14.

The most important effect of the field is the admixture of $|1_{s,a}>$ into the ground state. This causes Δ_ξ and Δ_η to increase, and the matrix elements M_ξ and M_η to decrease. The energies of the excita-

tions are thereby increased, while the dispersion becomes smaller. If the field is applied along the ξ-axis, the ξ-mode parameters are changed approximately twice as much, relative to their zero-field values, as the η-mode parameters. At $H = 43.5\,\mathrm{kOe}$, the total molecular field, which determines the energies in Fig. 7.12, is $100\,\mathrm{kOe}$, and $\Delta_\xi = 4.29\,\mathrm{meV}$, whereas $\Delta_\eta = 3.86\,\mathrm{meV}$. This means that the field produces the largest effects on the excitations polarized (predominantly) parallel to it, which in Fig. 7.14 are the transverse modes, both when $\mathbf{q}$ is along $\Gamma\mathrm{M}$ and along $\Gamma\mathrm{KM}$. The γ-strain coupling opposes the splitting of the transverse and longitudinal modes, but only quadratically in the field. The hexagonal anisotropy does not affect the effective $(J = 1)$-excitations in zero field, but B_6^6 causes a splitting between the $|3_\mathrm{S}>$ and $|3_\mathrm{a}>$-states of nearly $5\,\mathrm{meV}$. As B_6^6 is negative, the lower of the two states is $|3_\mathrm{S}>$ which, according to Fig. 1.16 or 7.12, should lie only $0.9\,\mathrm{meV}$ above the $|1_\mathrm{s,a}>$-states. The magnetic field induces a coupling between this neighbouring level and the doublet excitations, so that it acquires a significant scattering cross-section at the energies indicated by the dashed lines in Fig. 7.14. Although the extra peak was not sufficiently distinct to be detected directly in the neutron-scattering experiments, the presence of this level is clearly manifested in the behaviour of the doublet excitations. The absolute minimum in the excitation spectrum at zero field is found along $\Gamma\mathrm{M}$, whereas at $H = 43.5\,\mathrm{kOe}$ the energy minimum in the $\Gamma\mathrm{K}$-direction has become the lowest. The $|3_\mathrm{S}>$-excitations are coupled to the doublet excitations polarized along the ξ-axis, both when the field is along the ξ- and the η-axis. This means that the energy increase of the longitudinal (optical) mode in the $\Gamma\mathrm{K}$-direction is diminished, due to the repulsive effect of the field-induced coupling to the $|3_\mathrm{S}>$-excitations. When the field is along the ξ-direction, the longitudinal modes in the $\Gamma\mathrm{M}$-direction are coupled to the $|3_\mathrm{a}>$-excitations, which lie at much higher energies and only perturb the lower modes very weakly. The basal-plane anisotropy is also clearly reflected in the field dependence of the elastic constant c_{66}, shown in Fig. 7.5.

The effects of the field on the hexagonal doublet-excitations are very strong. In comparison with the zero-field result of Fig. 7.1, the minimum-energy modes have more than doubled their energies, while the overall width of the excitation bands has been reduced by nearly a factor of two. Because of these large changes, the measurement of the field dependence of the excitation spectrum allowed a rather precise determination of Δ and the relative position of the $|3_\mathrm{S}>$ crystal-field level. With the assumption that $B_6^6 = -(77/8)B_6^0$, these results then led to the crystal-field level-scheme for the hexagonal ions shown in Figs. 1.16 and 7.12, leaving only the position of the highest-lying level somewhat arbitrary. The field experiment also determined the value of

the magnetoelastic parameter $(B_{\gamma 2})^2/c_\gamma$. This agrees with the value of $B_{\gamma 2}$ for the hexagonal ions which accounts for the coupling between the magnetic excitations and the phonons, and for the field dependences of c_{66} (Fig. 7.5) and of the γ-strains (Hendy *et al.* 1979). It furthermore allowed the accurate prediction of the strain-induced antiferromagnetic transition in Pr, shown in Fig. 7.10.

The low-temperature magnetic properties of Pr are dominated by the hexagonal ions. One consequence of this is that it is more difficult to construct a reliable model for the cubic ions, based on experimentally derivable parameters. Although the model proposed by Houmann *et al.* (1979) accounts accurately for the bulk of the low-temperature experimental results, it is not uniquely specified and some deficiencies appear in comparison with experiments at elevated temperatures. The model is based on the following crystal-field Hamiltonian for the cubic ions:

$$
\mathcal{H}_J = \sum_{i \in \text{cub.ions}} \Big[B_4^0(c)\{O_4^0(\mathbf{J}_i) - 20\sqrt{2}\,O_4^{-3}(\mathbf{J}_i)\}
$$

$$
+ B_6^0(c)\{O_6^0(\mathbf{J}_i) + \frac{35}{4}\sqrt{2}\,O_6^{-3}(\mathbf{J}_i) - \frac{77}{8}O_6^6(\mathbf{J}_i)\} \Big],
$$

$$(7.4.6)$$

which neglects the departure of the local symmetry of these sites from cubic. We shall not present an extensive discussion of the model here (more details may be found in Houmann *et al.* (1979) and Jensen (1979b, 1982)), but it is clear that this MF model, which is the simplest description of Pr consistent with its magnetic behaviour in the low-temperature limit, must be extended in order to describe, for instance, the magnetostriction measurements of Hendy *et al.* (1979) and Ott (1975). In addition to introducing a non-zero value of $B_{\alpha 2}$ for the hexagonal ions, of the magnitude used to obtain agreement with experiment in Fig. 7.13, it is probably also necessary to include $B_{\alpha 1}$. Moreover, the magnetoelastic parameters for the cubic ions are presumably of the same order of magnitude as those on the hexagonal ions. This probably also applies to $B_2^0(c)$, neglected in eqn (7.4.6). The separation of the contributions from the hexagonal and the cubic ions to the c-axis bulk susceptibility as a function of temperature, accomplished through neutron-diffraction experiments by Rainford *et al.* (1981), indicates that not only is $B_2^0(c)$ nonzero, but the exchange between the c-axis components of the moments is also different from the corresponding coupling between the basal-plane components. The development of a MF model for Pr which describes its properties more accurately at elevated temperatures would benefit greatly from a more detailed examination of the excitations on the cubic sites, i.e. a determination of the energies of the excitations polarized in the c-direction, and the field-induced changes of these excitations, and of those polarized in the basal-plane and shown in Fig. 7.2.

The missing ingredients in the model presented here to describe Pr have a negligible influence on the pressure-induced ordered structure, and most of the observations made in this phase were explained by Jensen *et al.* (1987) utilizing only the information obtained from the zero-pressure studies of Houmann *et al.* (1979). Because the ordered moments in the antiferromagnetic phase are parallel to $\mathbf{Q}$, the change of the ground state affects primarily the longitudinal excitations, and the low-energy optical branch close to the ordering wave-vector is particularly strongly modified. Fig. 7.15 shows the experimental excitation energies of the optical modes in the ΓM-direction at 5.5 K, in the presence of a uniaxial pressure of 1.28 kbar, compared with the predictions of the RPA theory.

Under the conditions of the measurements, the analysis shows that the induced moments

$$\langle J_{i\eta}\rangle = \langle J_\eta(\mathbf{Q})\rangle \cos(\mathbf{Q}\cdot\mathbf{R}_i + \varphi) \qquad (7.4.7a)$$

are so small that the effective $(J = 1)$-model is adequate to describe the excitations, and the value of the third harmonic of the longitudinally ordered moments is only a few per cent of $\langle J_\eta(\mathbf{Q})\rangle$. A full account of the structure would require specifying two phase constants, one for
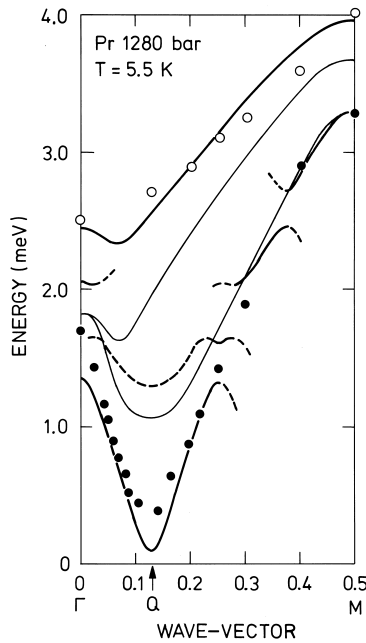

Fig. 7.15. The dispersion relations for the optical excitations in the antiferromagnetic phase of Pr at 5.5 K under an applied uniaxial pressure of 1.28 kbar. The ΓM direction shown is perpendicular to the pressure axis. The circles depict the experimental results obtained from inelastic neutron scattering, with solid and open symbols indicating the longitudinal and transverse branches respectively. The solid lines are the calculated RPA energies for the excitations, whereas the dashed lines indicate longitudinal modes of weaker intensity. The thin lines are the experimental dispersion relations in unstressed Pr, as in Fig. 7.1

each of the two sublattices. The difference between the two phases is approximately π, or approximately 0 if $\mathbf{Q}$, within the primitive zone, is replaced by $\mathbf{Q} + \mathbf{b}_3$. Introducing the relative magnetization σ by

$$\langle J_\eta(\mathbf{Q})\rangle = M_\eta\sigma, \qquad (7.4.7b)$$

where the matrix element is slightly dependent on the pressure ($M_\eta = 1.026\sqrt{10}$ at 1 kbar), we find that $\sigma \simeq 0.44$ under the conditions of Fig. 7.15. Because σ is still small, it may be utilized as an expansion parameter, both in the calculation of the ordered moments and also in the equations of motion determining the excitation spectrum. The ordering wave-vector is close to $\frac{1}{8}\mathbf{b}_2$, but whether the system is commensurable or not is not easy to decide from the experiments. In any case, this is not important for calculating the excitation spectrum, because distinctive effects of commensurability only appear in the order $\sigma^8 \approx 0.001$. The modulation of the length of the moments implies that the single-ion MF susceptibilty is site-dependent, and the $\eta\eta$-component is found to be

$$\chi^o_{\eta\eta}(j,\omega) = \frac{2n_{01}(j)M_\alpha^2\Delta\cos 2\theta_j}{(\Delta/\cos 2\theta_j)^2 - (\hbar\omega)^2} + \beta p_{01}(j)M_\alpha^2\sin^2 2\theta_j\,\delta_{\omega 0}, \quad (7.4.8a)$$

equivalent to eqn (7.1.9) with $\langle J_{j\eta}\rangle = M_\eta n_{01}(j)\sin(2\theta_j)$, and $p_{01}(j)$ defined by

$$p_{01}(j) = n_0(j) + n_1(j) - n_{01}^2(j). \qquad (7.4.8b)$$

$\Delta = \Delta_\eta(t_{11})$ is here the crystal-field splitting between the ground state $|0>$ and the excited state $|1> (\equiv |1_a>$ at zero stress) at the particular stress considered. In the incommensurable case, the coupling matrix determining the longitudinal component of the susceptibility tensor is of infinite extent. The situation is very similar to that considered in Section 6.1.2 and, as there, the coupling matrix may be solved formally in terms of infinite continued fractions. The only difference is that, in the present case, the single-site susceptibility is unchanged if the moments are reversed, which means that the coupling matrix only involves terms with n even (where n is the number of the Fourier component, as in (6.1.28)). Since the effective modulation wave-vector seen by the longitudinal excitations is $2\mathbf{Q}$ and not $\mathbf{Q}$, the acoustic and the optical modes propagating parallel to $\mathbf{Q}$ may be treated separately, as the $\mathbf{q}$-dependent phase factor determining the effective coupling parameters $\mathcal{J}_{11}(\mathbf{q}) \pm |\mathcal{J}_{12}(\mathbf{q})|$, derived from the interactions in the two sublattices (see Section 5.1), is not affected.

   To leading order, the modulation of the moments introduces a coupling between the excitations at wave-vectors $\mathbf{q}$ and $\mathbf{q}\pm 2\mathbf{Q}$, and energy gaps appear on planes perpendicular to $\mathbf{Q}$ passing through $n\mathbf{Q}$. When

$\mathbf{q} = \mathbf{Q}$, the coupling between the modes at $\mathbf{Q}$ and $-\mathbf{Q}$ leads to an *amplitude mode* and a *phason mode*, corresponding respectively to an in-phase and a 90° out-of-phase modulation of the lengths of the moments. The energies of the two longitudinal modes at $\mathbf{q} = \mathbf{Q}$ are approximately given by

$$E_{\text{amplitude}} \simeq \frac{\sqrt{3}}{2}\, \sigma\Delta$$
$$E_{\text{phason}} \simeq \left(\tfrac{1}{8}\beta\Delta\overline{p}_{01}\right)^{1/2}\sigma\Delta, \qquad\qquad (7.4.9)$$

where $\overline{p}_{01}$ is the average value of $p_{01}(j)$. The scattering intensity, proportional to $1/[\hbar\omega\{1 - \exp(-\beta\hbar\omega)\}]$, of the lowest-lying phason mode is much larger than that of the amplitude mode. The low-intensity amplitude mode is indicated by the dashed line at $\mathbf{q}$-vectors close to $\mathbf{Q}$ in Fig. 7.15, and it was not clearly resolved in the experiments. The phason mode has a dispersion relation, indicated by the solid lines in the figure, which increases linearly from the magnetic Bragg peak at $\mathbf{Q}$, except for the presence of the small gap E_{phason} at $\mathbf{q} = \mathbf{Q}$. In the incommensurable case, the free energy is invariant to a change of the phase constant φ in (7.4.7), so that the longitudinal component of the zero-frequency susceptibility diverges at the wave-vector $\mathbf{Q}$. The corresponding generator of an infinitesimal phase shift is $1 - i\delta\varphi\sum_j \left(|1 ><1|\right)_j$. If this generator commuted with the Hamiltonian, a specific choice of φ would break a continuous symmetry of the system, implying the presence of a well-defined linearly-dispersive Goldstone mode, as discussed in Section 6.1. However, as may be verified straightforwardly, it does not in fact commute with the Hamiltonian. On the contrary, within the RPA the longitudinal response contains an elastic contribution, due to the final term in (7.4.8*a*), and hence the scattering function contains a diffusive peak at zero frequency. It is the intensity of this peak which is found to diverge in the limit $\mathbf{q} \to \mathbf{Q}$. As $\mathbf{q}$ departs from $\mathbf{Q}$, the diffusive response at zero frequency rapidly weakens, and the phason mode begins to resemble a Goldstone mode. The presence of the inelastic phason mode at the wave-vector $\mathbf{Q}$ can be explained as a consequence of the modulation of the population difference $n_{01}(j)$, which is proportional to $\overline{p}_{01}$. This mode corresponds to an oscillation of the phase-constant φ in (7.4.7), except that the adiabatic condition, which applies within the RPA as soon as the oscillation frequency is non-zero, constrains $n_{01}(j)$ to remain constant, without participating in the oscillations. This condition, in turn, gives rise to the restoring force which determines the frequency of the oscillations. However, if the oscillations are so slow (i.e. essentially zero in the present approximation) that $n_{01}(j)$ can maintain its thermal-equilibrium value, there are no restoring forces. In the zero-temperature limit, $\overline{n}_1$ vanishes exponentially, in which case $n_{01}(j) = 1$, and the diffusive elastic response disappears together with E_{phason}. The

gap also vanishes in the other limit when $\sigma \to 0$, as does the amplitude-mode energy gap, reflecting the soft-mode nature of the transition in this approximation. In the above discussion, we have assumed that the system is incommensurable. In a commensurable structure, the free energy is no longer invariant to an overall phase shift of the structure, and the longitudinal susceptibility does not diverge at $\mathbf{Q}$. Because of the small value of σ^8, however, it is close to divergence. The phason-mode energy gap stays non-zero at $T = 0$ in the commensurable case, but it is estimated to be only about 0.03 meV at 1 kbar.

Even at the lowest temperatures reached in the inelastic neutron-scattering experiments, quite strong line-broadening of the low-lying longitudinal excitations was observed in the ordered phase. There are several mechanisms which may lead to non-zero linewidths. One possibility, if the ordering is incommensurable, is a broadening of the excitation peaks analogous to that illustrated in Fig. 6.3 in Section 6.1.2. However, the off-diagonal coupling terms, corresponding to γ_n in (6.1.30), are here multiplied by σ^2, which means that the continued-fraction solution, although infinite, converges very rapidly without producing linewidth effects of any importance. The $1/Z$-expansion, discussed in Section 7.2, accounts very well in first order in $1/Z$ for the lifetime effects observed in paramagnetic Pr, as shown in Fig. 7.4. In this order, the intrinsic-linewidth effects vanish exponentially at low temperature, and they should be negligible in the temperature range of the ordered phase, with the important exception that the elastic RPA response acquires a non-zero width. To first order in $1/Z$, $\delta_{\omega 0}$ in eqn (7.4.8a) is replaced by a Lorentzian $i\Gamma/(\hbar\omega + i\Gamma)$, with $1/\Gamma \simeq \overline{n}_{01}^2(\pi/2)\mathcal{N}_\eta(\Delta)$, where $\mathcal{N}_\eta(E)$ is the density of states of the η-polarized part of the excitation spectrum. Due to the large value of Γ, estimated to be about 1 meV, the RPA predictions for the behaviour of the phason modes near the ordering wave-vector are strongly modified. Instead of an elastic diffusive and an inelastic, adiabatic phason mode, the theory to this order predicts only one mode at zero energy, but with non-zero width, when $\mathbf{q}$ is close to $\mathbf{Q}$. An inelastic low-energy peak develops only at a distance of about $0.03|\mathbf{b}_1|$ from $\mathbf{Q}$. The exchange-enhancement factor in the scattering function causes the width of the Lorentzian near $\mathbf{Q}$ to be much less than 2Γ. Formally the width tends to zero when $\mathbf{q} \to \mathbf{Q}$, but it is more precisely the intensity which diverges, while strong inelastic tails remain at $\mathbf{q} = \mathbf{Q}$, in accordance with the experimental results.

As was mentioned in Section 7.2, the $1/Z$-expansion of the effective medium theory was extended to second order in $1/Z$ by Jensen *et al.* (1987). The second-order modifications are important here, but not in the zero-stress case considered in Fig. 7.4, because the low-temperature energy gap of about 1 meV in the excitation spectrum is suppressed by

the uniaxial pressure. The gapless excitation-spectrum in the ordered phase implies that the linewidth effects are predicted to vary smoothly with temperature, and to stay non-zero at $T = 0$, when the second-order contributions are included. We note that the imaginary part of the self-energy is now non-zero below the RPA-excitonic band in the paramagnetic phase, and that it generates an appreciable low-energy scattering at the ordering wave-vector, just above T_N, changing the inelastic critical excitation into a diffusive mode of diverging intensity. Hence a true 'soft-mode transition', as found in the zeroth or first order of $1/Z$, is no longer predicted, but the low-energy effect is far too weak to account for the observed behaviour of the neutron-diffraction satellite. The inclusion of the second-order effects in the theory clearly improves the agreement with the experimental results. However, even though the $1/Z^2$-theory predicts a non-zero linewidth in the limit $T \to 0$, the effect is so small, at energies below $1\,\mathrm{meV}$, that it can be neglected in comparison with the contribution due to the scattering against electron-hole pair excitations of the conduction electrons, discussed in Section 7.3.2. The importance of this mechanism has been estimated reasonably accurately, and it leads to a linewidth of the order of $0.15\,\mathrm{meV}$ for the optical modes close to $\mathbf{Q}$. When all contributions are included, the theory indicates that the amplitude mode should have been observable at $\mathbf{q} = \mathbf{Q}$ at the lowest temperatures, in contrast to the experimental results, but otherwise its predictions are found to agree well with the main features of the observations.